Petroleum Science 21 (2024) 836–854

Contents lists available at ScienceDirect

Petroleum Science

journal homepage: www.keaipublishing.com/en/journals/petroleum-science

Original Paper

The coupling control of biological precursors and environmental factors on β-carotane enrichment in alkaline lacustrine source rocks: A case study from the Fengcheng formation in the western Junggar Basin, NW China

Mao-Guo Hou [a], Ming Zha [a, *], Hua Liu [a, **], Hai-Lei Liu [b], Jiang-Xiu Qu [a], Ablimit Imin [b], Xiu-Jian Ding [a], Zhong-Fa Jiang [b]

[a] School of Geosciences, China University of Petroleum, Qingdao, Shandong, 266580, China
[b] Research Institute of Exploration and Development, Xinjiang Petroleum Administration Bureau, Karamay, Xinjiang, 834000, China

ARTICLE INFO

Article history:
Received 12 November 2022
Received in revised form
24 August 2023
Accepted 26 December 2023
Available online 1 January 2024

Edited by Jie Hao and Teng Zhu

Keywords:
β-carotane enrichment
Cyanobacterial input
Environmental impact
Alkaline lacustrine source rocks
The Fengcheng formation

ABSTRACT

The organic-rich mudstones and dolostones of the Permian Fengcheng Formation (Fm.) are typically alkaline lacustrine source rocks, which are typified by impressively abundant β-carotane. Abundant β-carotane has been well acknowledged as an effective indicator of biological sources or depositional environments. However, the specific biological sources of β-carotane and the coupling control of biological sources and environmental factors on the enrichment of β-carotane in the Fengcheng Fm. remains obscure. Based on a comprehensive investigation of the bulk, molecular geochemistry, and organic petrology of sedimentary rocks and the biochemistry of phytoplankton in modern alkaline lakes, we proposed a new understanding of the biological precursors of β-carotane and elucidated the enrichment mechanism of β-carotane in the Fengcheng Fm. The results show that the biological precursors crucially control the enrichment of β-carotane in the Fengcheng Fm. The haloalkaliphilic cyanobacteria are the primary biological sources of β-carotane, which is suggested by a good positive correlation between the 2-methylhopane index, 7- + 8- methyl heptadecanes/C_{max}, C_{29}%, and β-carotane/C_{max} in sedimentary rocks and the predominance of cyanobacteria with abundant β-carotene in modern alkaline lakes. The enrichment of β-carotane requires the reducing condition, and the paleoredox state that affects the enrichment of β-carotane appears to have a threshold. The paleoclimate conditions do not considerably impact the enrichment of β-carotane, but they have some influence on the water's paleosalinity by affecting evaporation and precipitation. While it does not directly affect the enrichment of β-carotane in the Fengcheng Fm., paleosalinity does have an impact on the cyanobacterial precursor supply and the preservation conditions.

1. Introduction

β-carotane, a fully saturated lipid with a β-carotene skeleton, have been frequently reported in numerous sedimentary rock and crude oil cases, for example, the Lower Cretaceous ultra-saline lacustrine strata in the Santos Basin, Brazil (Mello et al., 1993), the Permian organic-rich sediments from the Sudetes area, Poland (Yawanarajah et al., 1993), the Saline Fm. of the Lopare Basin, Bosnia and Herzegovina (Grba et al., 2014), the Lower Permian Irati Fm. of the Paraná Basin, Brazil (Martins et al., 2020), as well as the Fengcheng Fm. of the Junggar Basin, China (Ma et al., 2020; Wang et al., 2021; Xia et al., 2022; Zhang et al., 2022).

β-carotane was commonly interpreted as an indicator of biological sources (Moldowan et al., 1985; Peters et al., 2005; Ding et al., 2017), high salinity (Jiang and Fowler, 1986; Mello et al., 1993; Rippen et al., 2013), and reducing conditions (Peters et al., 2005; Ding et al., 2017). The biological input to organic matter (OM) of the Fengcheng Fm. was extensively investigated, but the results were ambiguous, showing that hydrobionts like algae and bacteria were the main biological input to OM (Chen et al., 2017;

* Corresponding author.
** Corresponding author.
E-mail addresses: mzha@upc.edu.cn (M. Zha), liuhua77@upc.edu.cn (H. Liu).

https://doi.org/10.1016/j.petsci.2023.12.019

Tang et al., 2021; Wang et al., 2021). Nevertheless, these investigations have not yet identified the specific biological source and established a direct connection between biological input and the enrichment of β-carotane. The research on the biological sources of β-carotane in the Fengcheng Fm. is relatively limited. According to Jiang and Fowler (1986) and Xia et al. (2022), the primary biological sources of β-carotane in the Fengcheng Fm. are carotene-rich algae and Dunaliella (green algae), respectively. However, these studies lack tangible evidence or a comprehensive analysis. The depositional environment indication of β-carotane in the Fengcheng Fm. has been well investigated. Previous studies stated that abundant β-carotane in the Fengcheng Fm. is an effective proxy for reducing (Gu, 2021; Wang et al., 2021) or/and hypersaline environments (Wang et al., 2017; Ma et al., 2020; Gu, 2021; Wang et al., 2021; Zhang et al., 2022). However, the mechanisms by which these environmental factors influence β-carotane in the Fengcheng Fm. are not yet clear. Therefore, the specific biological sources of β-carotane, as well as coupling control of biological precursors and environmental factors on β-carotane enrichment in the Fengcheng Fm., are still not well understood.

In this study, we combined the bulk and molecular geochemistry, organic petrology of sedimentary rocks in the Fengcheng Fm. with the biochemical analysis of phytoplankton in modern alkaline lakes to propose the primary biological sources of β-carotane and to elucidate how biological precursors and environmental factors interact to control the enrichment of β-carotane in the Fengcheng Fm. This investigation was expected to better understand the β-carotane-rich OM characteristics and the enrichment mechanism of β-carotane in alkaline lacustrine source rocks.

2. Geological setting

The study area is located in the western Junggar Basin, NW China (Fig. 1(a) and (b)). It contains the Mahu Sag, Kebai Fault Zone, Xiayan Fault Zone, Xiayan Uplift, Dabasong Uplift, and Zhongguai Uplift, covering an area of approximately 14,600 km^2. The study

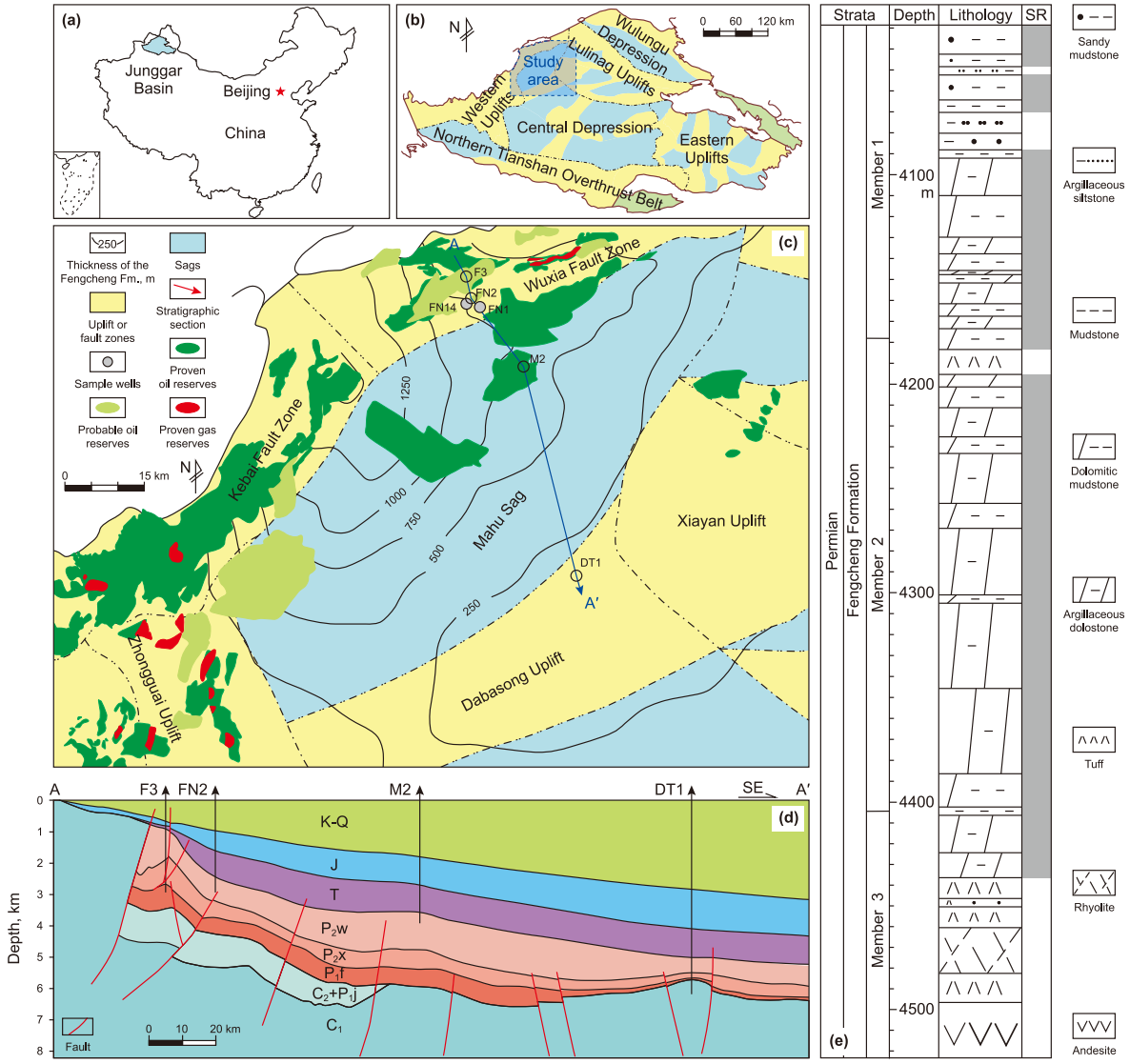

Fig. 1. Comprehensive geological maps showing the location of the Junggar Basin **(a)**, the location of the study area **(b)**, structural units, thickness of the Fengcheng Fm., oil and gas resource distribution in the study area **(c)**, the stratigraphic cross section of the western Junggar Basin **(d)**, and the strata, and lithology of the Fengcheng Fm. **(e)** (modified after Xia et al., 2020; Hou et al., 2022). C_1, C_2 = Lower, Upper member of Carboniferous System, T, J, K–Q = Triassic, Jurassic, Cretaceous to Quaternary systems, P_2w = Permian Wuerhe Fm., P_2x = Permian Xiazijie Fm., P_1f = Permian Fengcheng Fm., P_1j = Permian Jiamuhe Fm.; SR = source rock.

area is the most petroliferous area in the Junggar Basin, with substantial oil and gas reserves (Fig. 1(c)).

The western Junggar Basin possesses sedimentary strata ranging from Permian to Quaternary systems with a Carboniferous volcanic basement (Fig. 1(d)). The target stratum, "the Fengcheng Fm.," has a huge thickness (Fig. 1(c)), and was proved to be the primary source of oil and gas resources in the western Junggar Basin (Ma et al., 2020; Wang et al., 2021; Hou et al., 2022; Zhang et al., 2022), yielding billions of tons of oil and gas reserves in the western Juggar Basin, NW China (Xia et al., 2022). The Fengcheng Fm. was deposited in a Paleozoic alkaline lake in the geological times of 305–207 Ma ago (Xia et al., 2020; Hou et al., 2022). The Fengcheng Fm. can be separated into three members (Mbr.) from bottom to top (i.e., members 1, 2, and 3), consisting of bottom volcanic rocks (e.g., andesite, rhyolite, and tuff) and an overlying sedimentary rock assemblage of mudstone, dolomite mudstone, sandy mudstone, and argillaceous dolostone (Fig. 1(e)).

3. Samples and methods

3.1. Samples

A total of 61 drilling core samples (see Fig. 2) from two wells were collected to measure total organic carbon (TOC), Rock-Eval analysis, and gas chromatography-mass spectrometry (GC-MS). The well location distribution of samples is shown in Fig. 1(c), and the specific information about samples is listed in Table 1.

3.2. Analytical methods

3.2.1. TOC, sulfur content, and Rock-Eval analysis

TOC, sulfur content, and Rock-Eval measurements were carried out to describe the geochemical characteristics of the Fengcheng Fm. source rocks. Rock samples were crushed to a 100-mesh size for TOC and Rock-Eval measurements. Before TOC measurements, rock powders were put in a 6 mol/L HCl solution for 24 h to remove carbonates. TOC and sulfur content of 200 mg powders were measured in a LECO CS-230 analyzer. Rock-Eval 6 equipment employed 100 mg rock powders to measure free (S_1) and cracked (S_2) hydrocarbons as well as the temperature at which the maximum hydrocarbon production rate occurred (T_{max}). The temperature was initially set at 300 °C and maintained there for 3 min to quantify the S_1 peak response. Then the temperature was raised to 600 °C, holding for 1 min to obtain S_2 and T_{max}.

3.2.2. GC-MS

When source rock samples are contaminated by foreign hydrocarbons, the pyrolysis data of the samples typically exhibit $S_1 > S_2$. Hence, rock samples with $S_1 > S_2$ were excluded from GC-MS measurements to minimize potential contamination from foreign hydrocarbons. The core samples were crushed into a 100-mesh size. The rock powders were extracted in a Soxhlet extractor by utilizing an 8:2 vol ratio mixture of CH_2Cl_2 and CH_3OH for 48 h to gain bitumen. The bitumen's polar, saturated, and aromatic hydrocarbon fractions were separated by using dry-packed silica gel column chromatography. An Agilent 7890GC/5975iMS equipped with an HP-5MS (30 m × 0.25 mm × 0.25 μm) was used to conduct the gas chromatography-mass spectrometry (GC-MS) of the saturated hydrocarbons. The GC-MS system was configured with an EI mode and a 70 Ev current. The carrier gas (99.999% helium) flowed at a rate of 1 mL/min. The initial temperature was set at 50 °C and held for 1 min. Then it was increased to 120 °C at a rate of 20 °C per minute and to 310 °C at a rate of 3 °C per minute and kept there for 30 min. To eliminate potential background signals from the sample's biomarker, crushed pre-combusted sand (heated at 750 °C for 12 h) was measured following the same analytical procedures as the sample powders. The abundance of any high biomarker signals in the samples was at least four orders of

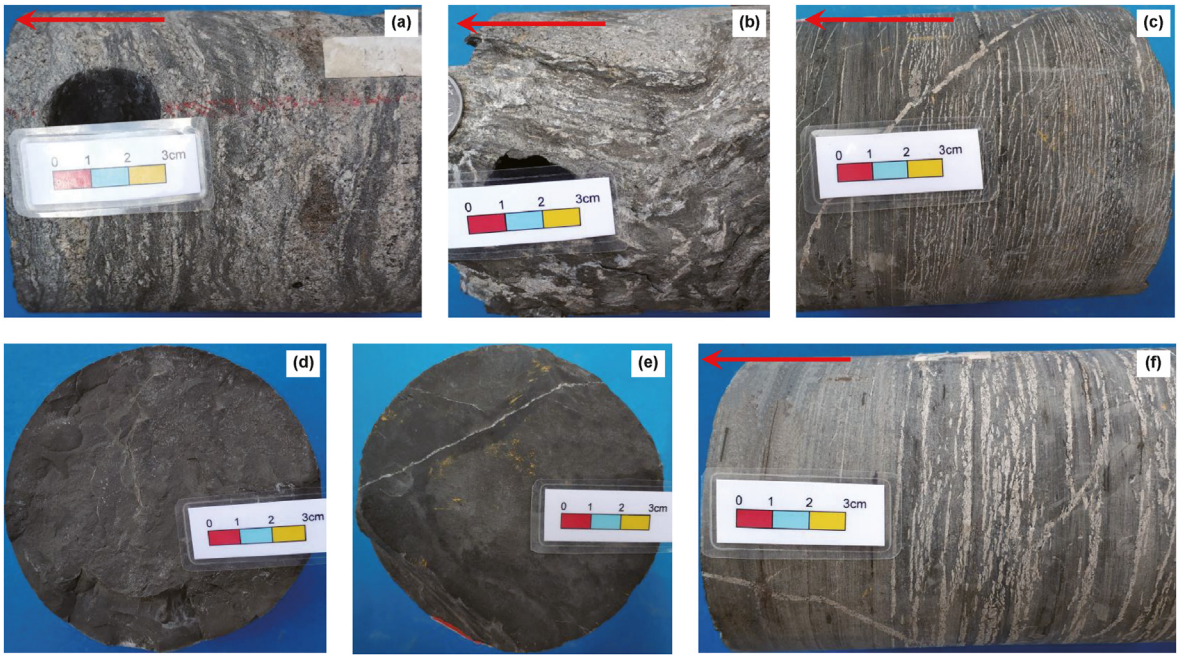

Fig. 2. Typical photos of the Fengcheng Fm. core samples. **(a)**. FN14, 4111.16–4122.74 m, dolomitic mudstone; **(b)**. FN14, 4174.25–4183.16 m, dolomitic mudstone; **(c)**. FN1, 4197.35–4207.83 m, dolomitic mudstone; **(d)**. FN1, 4210.44 m, argillaceous dolostone; **(e)**. FN1, 4361.38 m, argillaceous dolostone; **(f)**. FN1, 4369.12–4382.35 m, dolomitic mudstone; The red arrow points to the top of the core.

Table 1
Total organic carbon, Rock-Eval pyrolysis, biomarker, major element parameter data from source rocks in the Fengcheng Fm.

Well	Depth	Strata	Lithology	TOC, %	S_1, mg/g	S_2, mg/g	S_1+S_2, mg/g
FN14	4035.46	Mbr. 3	AD	1.7	2.60	5.83	8.43
FN14	4036.88	Mbr. 3	AD	0.54	0.18	0.32	0.5
FN14	4058.17	Mbr. 3	DM	1.14	0.10	3.69	3.79
FN14	4061.35	Mbr. 3	DM	0.8	1.38	3.18	4.56
FN14	4062.98	Mbr. 3	DM	2.89	2.20	19.77	21.97
FN14	4064.75	Mbr. 3	DM	2.31	0.70	13.93	14.63
FN14	4076.63	Mbr. 3	DM	1.22	0.90	5.44	6.34
FN14	4077.28	Mbr. 3	DM	1.85	2.53	6.06	8.59
FN14	4077.98	Mbr. 3	DM	0.99	0.14	3.22	3.36
FN14	4079.05	Mbr. 3	AD	0.39	0.05	1.11	1.16
FN14	4081.88	Mbr. 3	DM	1.01	0.06	3.52	3.58
FN14	4083.65	Mbr. 3	DM	0.63	0.28	1.31	1.59
FN14	4084.76	Mbr. 3	DM	0.68	0.09	1.88	1.97
FN14	4085.07	Mbr. 3	DM	1.84	1.59	8.66	10.25
FN14	4088.93	Mbr. 3	DM	1.15	0.06	3.23	3.29
FN14	4094.25	Mbr. 3	AD	1.94	2.95	11.13	14.08
FN14	4094.68	Mbr. 3	AD	0.88	0.14	2.47	2.61
FN14	4095.44	Mbr. 3	DM	0.88	0.32	2.00	2.32
FN1	4097.95	Mbr. 3	DM	0.88	0.11	3.76	3.87
FN14	4103.19	Mbr. 3	AD	0.60	0.01	1.74	1.75
FN14	4105.93	Mbr. 3	AD	0.56	0.06	1.25	1.31
FN14	4107.33	Mbr. 3	DM	1.05	0.14	3.66	3.80
FN14	4110.05	Mbr. 3	AD	0.64	0.04	1.31	1.35
FN14	4111.16	Mbr. 3	DM	1.11	0.70	2.94	3.64
FN1	4122.85	Mbr. 3	DM	0.89	0.10	2.11	2.21
FN1	4125.08	Mbr. 3	DM	0.98	0.43	3.18	3.61
FN1	4153.46	Mbr. 3	DM	0.87	0.13	2.85	2.98
FN14	4162.02	Mbr. 3	DM	1.72	1.81	5.40	7.21
FN14	4163.29	Mbr. 3	DM	0.51	0.09	0.95	1.04
FN14	4164.17	Mbr. 3	AD	1.36	0.06	3.33	3.39
FN14	4164.34	Mbr. 3	DM	1.63	0.14	7.71	7.85
FN14	4165.58	Mbr. 3	DM	1.47	0.10	12.48	12.58
FN14	4166.41	Mbr. 3	AD	1.80	0.29	11.41	11.70
FN14	4167.42	Mbr. 3	DM	0.82	0.93	3.18	4.11
FN14	4168.42	Mbr. 3	AD	0.49	0.07	0.92	0.99
FN14	4168.93	Mbr. 3	AD	1.12	1.71	4.51	6.22
FN14	4171.96	Mbr. 3	AD	0.61	0.16	1.26	1.42
FN14	4172.71	Mbr. 3	AD	1.05	0.03	2.14	2.17
FN14	4174.25	Mbr. 3	DM	0.55	0.30	1.54	1.84
FN1	4181.36	Mbr. 3	DM	0.45	0.16	1.10	1.26
FN1	4184.86	Mbr. 3	DM	0.70	0.25	1.86	2.11
FN1	4197.35	Mbr. 3	DM	1.16	2.74	4.14	6.88
FN1	4210.44	Mbr. 2	AD	0.51	0.19	1.37	1.56
FN1	4213.87	Mbr. 2	AD	1.44	0.21	5.93	6.14
FN1	4231.69	Mbr. 2	DM	0.80	0.23	2.89	3.12
FN1	4234.56	Mbr. 2	DM	0.70	0.25	1.94	2.19
FN1	4238.66	Mbr. 2	AD	0.98	2.57	3.06	5.63
FN1	4239.46	Mbr. 2	AD	0.81	0.62	2.57	3.19
FN1	4253.63	Mbr. 2	AD	0.88	0.15	3.15	3.30
FN1	4254.84	Mbr. 2	AD	0.56	0.06	2.00	2.06
FN1	4322.67	Mbr. 2	AD	0.69	0.34	2.17	2.51
FN1	4323.58	Mbr. 2	AD	0.84	0.81	2.73	3.54
FN1	4330.12	Mbr. 2	AD	0.56	0.08	1.72	1.80
FN1	4340.45	Mbr. 2	AD	1.85	0.16	11.51	11.67
FN1	4342.22	Mbr. 2	AD	1.21	0.07	4.02	4.09
FN1	4361.38	Mbr. 2	AD	0.51	0.09	1.35	1.44
FN1	4367.88	Mbr. 2	DM	0.93	1.01	2.93	3.94
FN1	4369.12	Mbr. 2	DM	0.86	0.12	2.03	2.15
FN1	4422.65	Mbr. 1	DM	0.88	1.99	2.66	4.65
FN1	4423.05	Mbr. 1	DM	0.69	0.05	2.89	2.94
FN1	4443.56	Mbr. 1	DM	0.64	1.15	2.08	3.23

Well	HI, mg/g TOC	T_{max}, °C	A	B	C	D	E	F	G	H
FN14	342.94	433	0.46	1.22	0.06	0.24	0.52	48.66	/	2.60
FN14	59.26	435	0.63	1.05	0.14	0.22	0.66	42.83	/	2.96
FN14	323.68	445	1.39	0.73	0.19	0.28	0.47	56.75	/	3.50
FN14	397.50	435	0.53	1.10	0.13	0.17	0.63	47.63	/	1.51
FN14	684.08	445	0.74	1.11	0.24	0.15	0.64	51.56	12.22	1.81
FN14	603.03	442	0.69	1.15	0.24	0.19	0.61	54.79	/	1.30
FN14	445.90	436	0.65	1.01	0.15	0.36	0.53	50.50	/	1.50
FN14	327.57	436	0.37	1.01	0.19	0.32	0.58	49.55	/	3.04
FN14	325.25	444	0.58	0.93	0.14	0.31	0.43	53.04	8.15	1.24
FN14	284.62	444	0.38	0.92	0.12	0.26	/	47.97	/	6.44

(*continued on next page*)

Table 1 (*continued*)

Well	HI, mg/g TOC	T_{max}, °C	A	B	C	D	E	F	G	H
FN14	348.51	448	0.58	1.00	0.19	0.32	0.55	50.89	5.08	0.63
FN14	207.94	438	0.33	0.95	0.09	0.41	0.59	45.57	/	/
FN14	276.47	441	0.83	0.90	0.20	0.31	0.59	49.86	/	0.74
FN14	470.65	438	0.68	1.05	0.15	0.26	0.61	52.77	/	0.56
FN14	280.87	442	1.03	0.94	0.10	0.25	0.60	53.31	7.85	/
FN14	573.71	438	2.17	0.95	0.13	0.21	0.57	58.04	/	1.76
FN14	280.68	442	1.82	0.91	0.19	0.15	0.52	58.41	/	1.00
FN14	227.27	435	0.86	1.00	0.16	0.21	0.49	52.63	/	/
FN1	427.27	438	4.88	0.92	0.19	0.17	0.55	59.73	/	1.16
FN14	290.00	448	0.67	0.83	0.13	0.26	0.59	54.97	/	/
FN14	223.21	441	0.50	0.83	0.14	0.33	0.49	46.13	/	0.96
FN14	348.57	444	0.46	1.00	0.28	0.36	0.50	48.74	/	0.48
FN14	204.69	443	0.91	0.98	0.26	0.30	0.59	51.57	/	/
FN14	264.86	442	0.44	1.11	0.17	0.28	0.86	48.28	/	0.67
FN1	237.08	442	0.62	0.75	0.12	0.25	0.56	48.76	/	2.33
FN1	324.49	441	0.48	0.98	0.22	0.38	0.53	47.67	7.63	0.62
FN1	327.59	438	2.26	0.61	0.14	0.19	0.64	56.76	/	/
FN14	313.95	442	1.55	0.82	0.15	0.39	0.84	57.30	/	0.88
FN14	186.27	438	0.97	0.66	0.18	0.46	0.81	52.48	/	/
FN14	244.85	443	0.43	0.81	0.12	0.53	0.79	48.57	/	/
FN14	473.01	444	1.39	0.84	0.24	0.35	0.61	49.43	/	1.15
FN14	848.98	450	0.79	0.82	0.15	0.41	0.75	55.11	/	1.19
FN14	633.89	440	0.71	0.83	0.24	0.40	0.76	54.31	/	/
FN14	387.80	439	0.28	0.73	0.12	0.48	0.74	45.94	/	0.32
FN14	187.76	437	0.45	0.68	0.09	0.49	0.69	48.97	5.24	/
FN14	402.58	449	0.35	0.70	0.09	0.65	0.73	38.93	/	0.54
FN14	206.56	444	0.45	0.64	0.10	0.56	0.70	50.66	6.67	/
FN14	203.81	449	0.30	0.73	0.08	0.54	0.75	37.93	4.78	0.42
FN14	280.00	437	0.39	0.63	0.09	0.47	0.71	48.55	/	0.33
FN1	244.44	437	0.50	0.63	0.06	0.51	0.66	47.64	7.63	/
FN1	265.71	437	0.35	0.67	0.13	0.55	0.81	48.35	/	0.37
FN1	356.77	439	0.24	0.61	0.15	0.57	0.82	47.46	/	0.36
FN1	268.63	435	0.32	0.59	0.12	0.61	0.95	48.79	/	0.74
FN1	411.81	439	1.28	0.61	0.20	0.36	0.81	57.03	11.21	0.92
FN1	361.25	440	0.35	0.58	0.12	0.63	0.79	47.67	/	0.46
FN1	277.14	437	0.24	0.55	0.09	0.71	0.79	45.45	3.91	0.26
FN1	312.56	444	2.44	0.61	0.15	0.30	1.00	56.14	15.12	/
FN1	317.28	436	1.72	0.73	0.26	0.35	0.97	56.28	7.12	0.92
FN1	357.95	435	2.18	0.67	0.21	0.49	0.88	55.03	9.54	0.51
FN1	357.14	441	1.96	0.78	0.23	0.51	0.91	56.83	/	/
FN1	314.49	437	1.92	0.65	0.33	0.69	0.99	56.89	12.81	0.24
FN1	325.36	437	2.25	0.52	0.28	0.63	0.96	57.55	/	0.54
FN1	307.14	435	5.57	0.60	0.34	0.51	0.92	62.83	/	/
FN1	622.16	442	1.28	0.79	0.15	0.61	/	51.17	8.05	0.52
FN1	332.23	440	1.53	0.70	0.23	0.63	0.76	51.11	/	0.32
FN1	264.71	434	5.04	0.62	0.32	1.28	0.80	62.34	19.22	0.19
FN1	315.05	433	4.90	0.90	0.51	1.71	0.85	58.25	/	0.11
FN1	236.05	432	6.43	0.67	0.42	1.78	0.87	64.21	23.14	0.48
FN1	302.46	436	1.97	0.83	0.20	0.57	0.89	52.86	/	/
FN1	418.84	446	2.45	0.68	0.15	0.55	0.84	51.06	12.45	0.63
FN1	325.26	442	1.23	0.52	0.23	0.81	0.89	54.47	/	/

DM = dolomitic mudstone; AD = argillaceous dolostone; TOC = total organic carbon; S_1 = free hydrocarbon; S_2 = cracked hydrocarbon; T_{max} = temperature of maximum hydrocarbon generation rate; HI = hydrogen indix = S_2/TOC × 100; A. β-carotane/C_{max}, C_{max} = the dominant normal alkane in TIC; B. Pr/Ph = pristane/phytane; C. 7- + 8-methyl heptadecanes/C_{max}; D. Gam/C_{30}H = gammacerane/C_{30} 17α, 21β(H)-hopane; E. C_{35}H/C_{34}H=C_{35} homohopanes (22S + 22R)/C_{34} homohopanes (22S + 22R); F. C_{29}% = C_{29} steranes/sum (C_{27}–C_{29} steranes) × 100; G. 2-methylhopane index (2-MHI); H. C/S = organic carbon/sulfur element of rock sample.

magnitude higher than that in the procedural blanks.

3.2.3. Kerogen maceral analysis

Kerogen maceral analysis includes kerogen isolation and identification of kerogen macerals, which follows isolation method for kerogen from sedimentary rock (General Administration of Quality SupervisionInspection and Quarantine, 2010) and the method of identification microscopically the macerals of kerogen and indivision the kerogen type by transmitted-light and fluorescence (National Energy Administration, 2015). 90 g source rock samples were crushed to a 100-mesh size. The powdered rock sample was soaked in distilled water for 4 h. Step 1: Concentrated hydrochloric acid with a concentration of 6 mol/L was added to the sample at a ratio of 8 mL/g, and stirred for 2 h at 70 °C. Step 2: Remove the acid solution, wash the sample with distilled water until weakly acidic, and then remove the clear liquid. Step 3: Concentrated hydrochloric acid with a concentration of 6 mol/L and hydrofluoric acid with a concentration of 40% were added to the sample at ratios of 2.4 mL/g and 3.6 mL/g respectively, and stirred for 2 h at 70 °C. Step 4: Wash the sample three times with 1 mol/L hydrochloric acid, then remove the clear liquid. Step 5: Steps 1 and 4 were repeated. Step 6: Steps 3 and 4 were repeated. Step 7: Steps 1, 4, and 2 were repeated. Step 8: Add a heavy liquid with a density of 8 g/mL to the obtained kerogen, then centrifuge at 3000 rpm for 20 min. Remove the upper

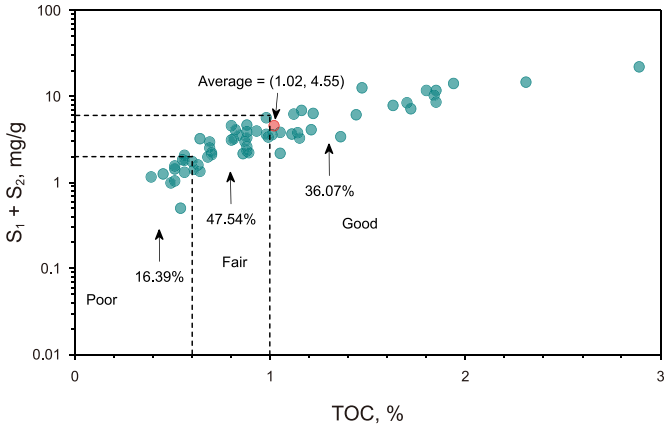

Fig. 3. TOC versus $S_1 + S_2$ of samples showing organic matter abundance of the Fengcheng Fm.

kerogen after layering, and repeat this step three times. Step 9: Freeze the obtained kerogen at −5 °C for 6 h, then dry it in a 50 °C drying oven. Step 10: Clean the kerogen with chloroform to remove soluble organic matter. Step 11: Take a 15 mg kerogen sample and place it in a high-temperature furnace, incinerate at 800 °C for 1 h, and weigh it after cooling for 30 min. Repeat this step until the weight change is within ±0.2 mg range. Step 12: Calculate the charred loss of the kerogen, which should be greater than 75%.

After preparing the kerogen, grind it into thin slices and prepare them as thin sections using a resin binder. Observe the thin sections under a fluorescence microscope. Kerogen macerals are classified into sapropelinite, exinite, vitrinite, and inertinite based on their type, color, and fluorescence characteristics (National Energy Administration, 2015). Sapropelinite further comprises planktonic alginite and sapropelic amorphogen, while exinite encompasses resinite, suberinite, cutinite, sporopollenite, fungal sporinite, humic amorphogen, and benthic algal elmorphogen. Vitrinite is divided into perhydrous vitrinite and normal vitrinite, whereas inertinite primarily consists of fusinite (National Energy Administration, 2015).

4. Results

4.1. Bulk geochemical characteristics of the Fengcheng Fm

The organic-rich dolomitic mudstone, argillaceous dolostone, and mudstone of the Lower Permian Fengcheng Fm. have been

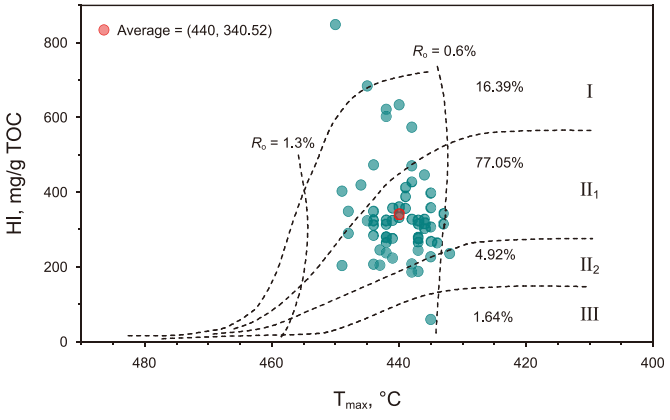

Fig. 4. T_{max} versus HI of samples showing organic matter type of the Fengcheng Fm.

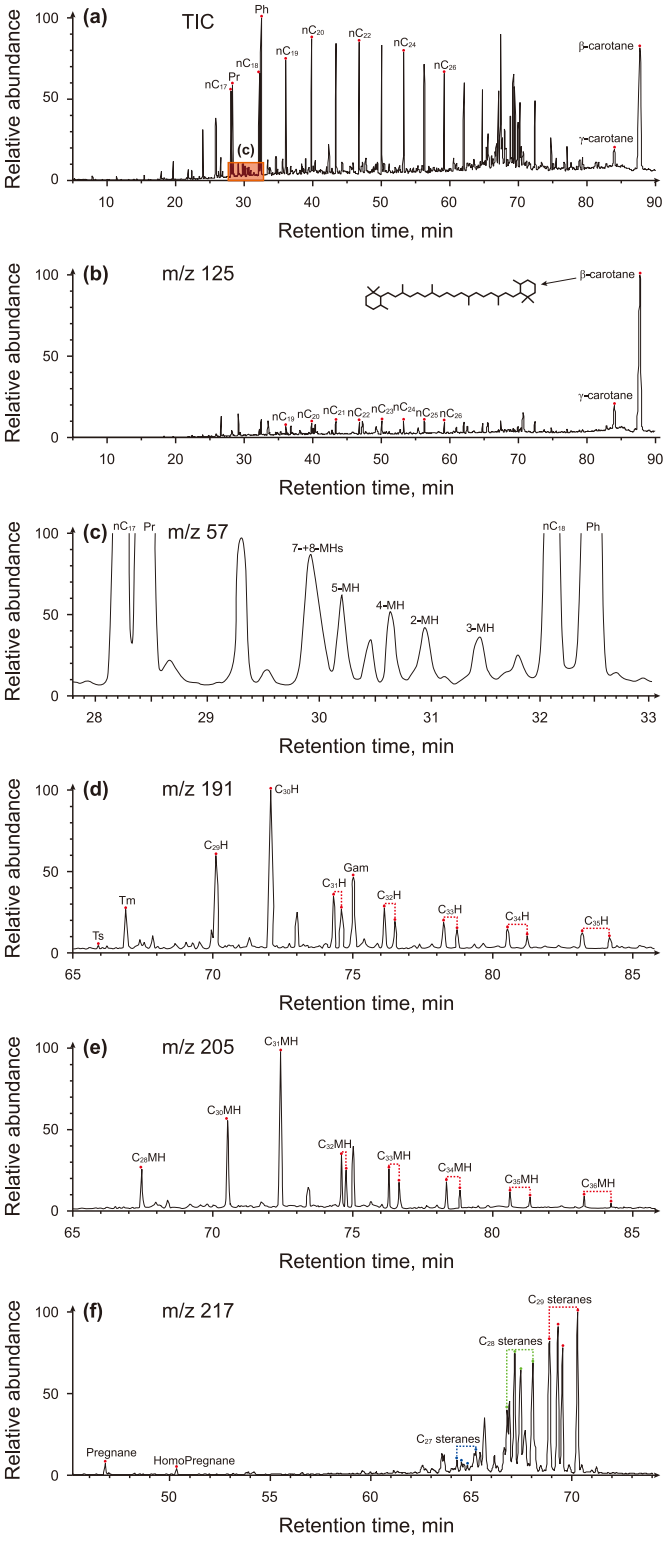

Fig. 5. Total ion chromatogram (TIC) **(a)**, m/z 125 **(b)**, m/z 57 **(c)**, m/z 191 **(d)**, m/z 205 **(e)**, and m/z 217 **(f)** mass chromatograms showing the distribution of normal alkanes, isoalkanes, β-carotane, terpanes, hopanes, and steranes, respectively. nC_i = normal alkane with carbon number of *i*; Pr = pristane; Ph = phytane; 7- + 8-MHs = 7- + 8-methyl heptadecanes; *i*-MH = *i*-methyl heptadecane, *i* = the carbon number that the methyl branch is located; C_i TT = tricyclic terpene with carbon number of *i*; C_i H = hopane with carbon number of *i*; Gam = gammacerane; C_i MH = 2-methylhopane with carbon number of *i*.

previously identified as the primary source rocks for considerable proven resource reserves (Hou et al., 2022; Xia et al., 2022). In this study, TOC and Rock-Eval pyrolysis are used to assess the OM abundance of the Fengcheng Fm., as shown in Fig. 3. The TOC values of source rocks range from 0.39% to 2.89%, with an average of 1.02%. The minimum, maximum, and average values of $S_1 + S_2$ are 0.50, 21.97, and 4.55 mg/g TOC, respectively. As a whole, the proportions of the fair and good source rocks are 47.54% and 36.07%, indicating the high abundance of OM in the Fengcheng Fm. The hydrocarbon generation potential indices (HI) display a scattered distribution with a minimum of 59.26 mg/g TOC, a maximum value of 848.98 mg/g TOC, and an average of 340.52 mg/g TOC (Fig. 4). Overall, 16.39% and 77.05% of HI values fall into type I or II_1 categories of OM, respectively, which readily generate oil with a T_{max} value range of 432–450 °C, an average of 440 °C, and an equivalent vitrinite reflectance range of 0.6%–1.1% (Fig. 4).

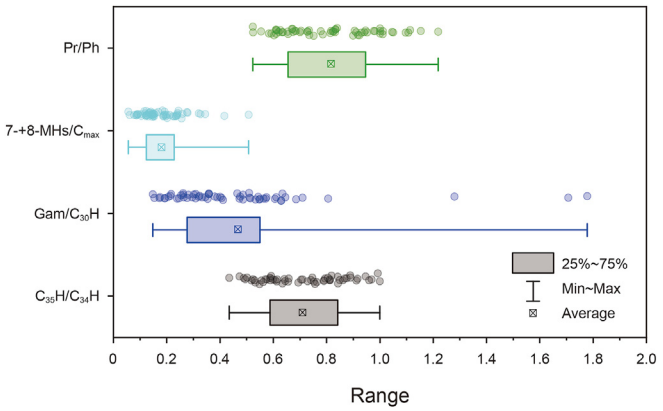

Fig. 7. The ranges of biomarker parameters showing biological input and paleo-environment of the Fengcheng Fm.

4.2. β-carotane

High abundances of β-carotane were identified in the Fengcheng Fm.'s samples using the total ion chromatogram (TIC) (Fig. 5(a), more GC-MS diagrams can been seen in Figs. S1–S5). Sometimes, β-carotane outcompetes all compounds to be the peak component in TIC. The m/z 125 mass chromatogram of saturated hydrocarbons can well illustrate the distribution of carotanes (Fig. 5(b)). The β-carotane index (i.e., the ratio of β-carotane and the dominant normal alkane (C_{max}) in TIC) was commonly used to reveal the abundance of β-carotane in sediments (Ding et al., 2017, 2020). The range of β-carotane indices is from 0.24 to 6.43, with a median value of 0.71, and an average value of up to 1.31. 10%–90% of total samples have β-carotane indices ranging from 0.35 to 2.44 (Fig. 6).

4.3. Other biomarkers

4.3.1. Isoalkanes

Pristane (Pr) and phytane (Ph) are mostly converted from the phytyl side chain of chlorophyll in photosynthetic organisms (Peters et al., 2005). A reducing condition in sediments facilitates the conversation of phytane from the phytyl side chain, while pristane is readily yielded under an oxidizing condition (Peters et al., 2005; Brocks and Schaeffer, 2008). Therefore, the Pr/Ph ratio is an effective proxy for the redox condition of the depositional water column, which typically implies reducing and oxidizing conditions with Pr/Ph < 1, and > 1, respectively (Ding et al., 2017; Hou et al., 2022). Phytane has a clear predominance over pristane (Fig. 5(a)). The Fengcheng Fm.'s Pr/Ph values range from 0.52 to 1.22, with an average of 0.81, suggesting deposition in a strongly reducing water environment (Fig. 7).

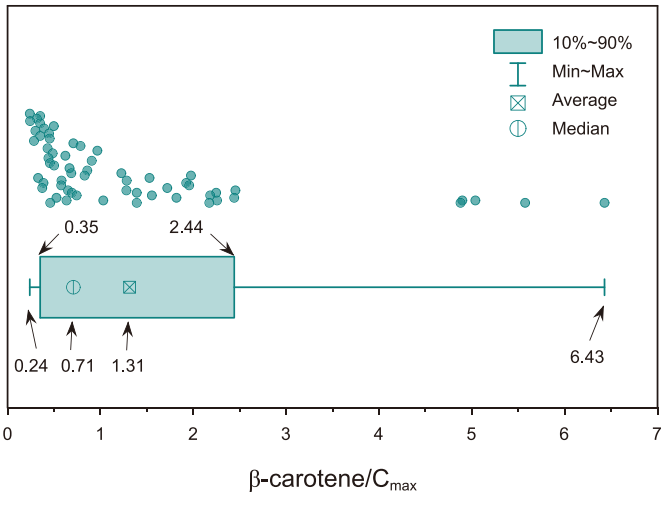

Fig. 6. The range of β-carotane/C_{max} showing high abundance of β-carotane in the Fengcheng Fm.

Middle-chain monomethyl alkanes, particularly 7- and 8-methyl heptadecanes (7- + 8-MHs), are prevalent in modern cultured cyanobacteria, predominant cyanobacteria in blooms, and cyanobacteria-rich sediments (Peters et al., 2005; Ding et al., 2020). The 7- + 8-MHs predominate over their 2-, 3-, 4-, 5-, and 6-methyl homologs in the Fengcheng Fm. (Fig. 5(c)). The ratio of 7- + 8-MHs/C_{max} (C_{max} is the dominant normal alkane in the m/z 57 mass chromatogram) was used to reflect the abundance of 7- + 8-MHs. The 7- + 8-MHs/C_{max} ratios range from 0.06 to 0.51 with an average of 0.18, and 25%–75% of samples have a range of 0.12–0.23 (Fig. 7).

4.3.2. Hopanes and 2-methylhopanes

Abundant C_{29}–C_{35} hopanes were detected in the m/z 191 mass chromatogram, with C_{30} 17α, 21β(H)-hopane as the peak compound (Fig. 5(d)). Gammacerane is suggested to be transformed from tetrahymanol, which biologically originates from organisms that prefer to grow at the boundary between oxidizing and reducing zones in a stratified water column (Sinninghe Damste et al., 1995; Ding et al., 2017). Consequently, the high abundance of gammacerane was frequently used to signify the water column stratification that is typically caused by hypersalinity and temperature gradients (Peters et al., 2005). In the Fengcheng Fm., the gammacerane index (i.e., Gam/C_{30}H = gammacerane/C_{30} 17α,21β(H)-hopane) is generally large, ranging from 0.15 to 1.78 with an average of 0.46 (Fig. 7). Previous investigations have demonstrated that high abundances of C_{35} homohopanes are typically associated with anoxic environments, and the C_{35} homohopane index (i.e., C_{35}H/C_{34}H=C_{35} homohopanes (22 S + 22 R)/C_{34} homohopanes (22 S + 22 R)) is an indicator of redox conditions (Schouten et al., 1995; Peters et al., 2005). The C_{35}H/C_{34}H ratio has a minimum of 0.43, a maximum of 1.00, and an average of 0.71 (Fig. 7).

Previous investigations demonstrated that 2-methylhopanepolyols, which are abundant in cyanobacteria, can be converted into 2-methylhopanes (2-MHs) during sedimentary diagenesis (Summons et al., 1999; Hou et al., 2022). Therefore, 2-MHs are remarkably effective at assessing cyanobacteria's contribution to OM in sediments, which is commonly represented

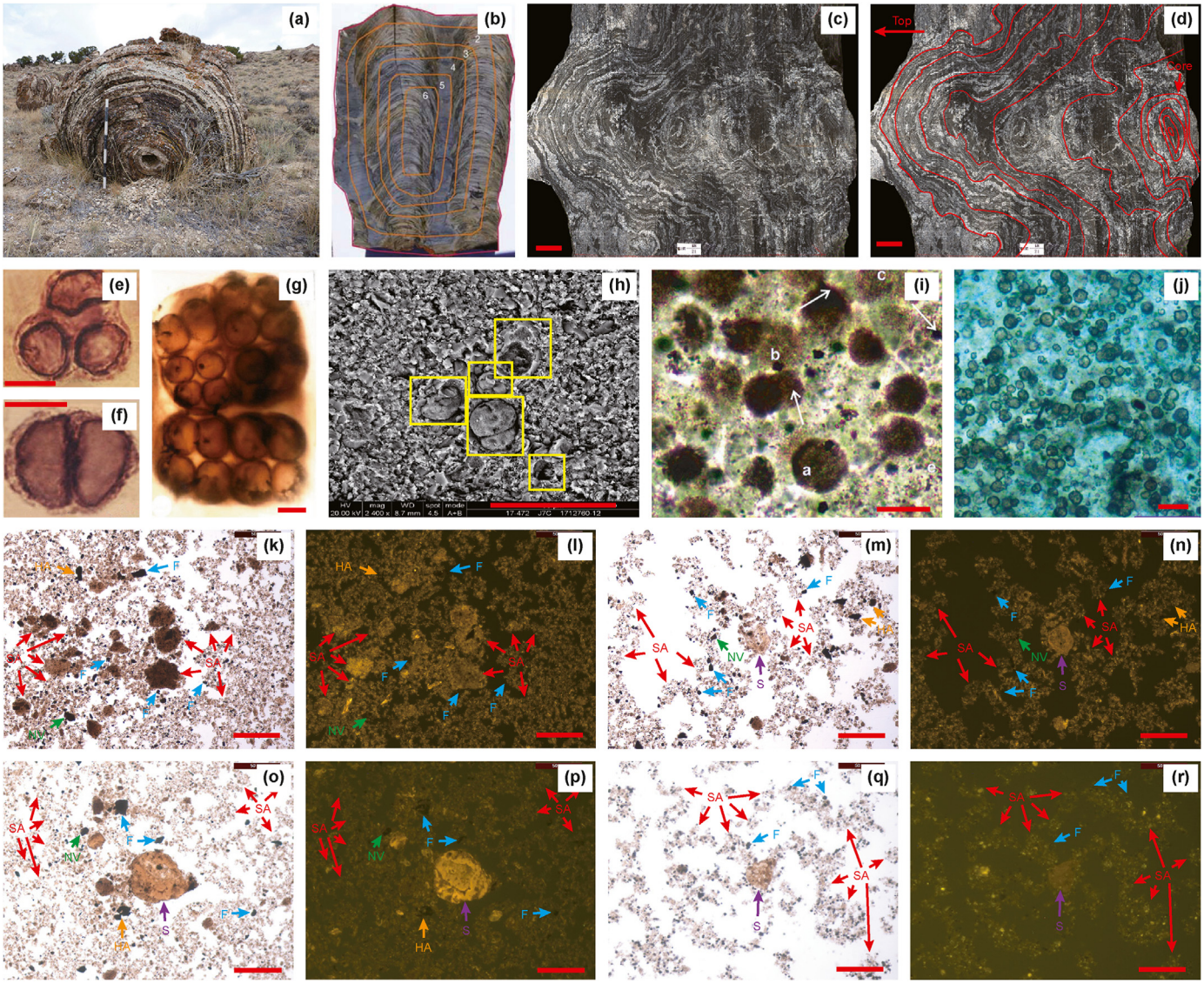

Fig. 8. Stromatolites, microbial fossils of cyanobacteria, and kerogen maceral in Precambrian, the Green River Fm., and the Fengcheng Fm. ancient sediments. **(a)**. Giant stromatolite from an outcrop of the Green River Fm., Colorado, USA; **(b)**. Stromatolites of the Tumbiana Fm., Fortescue Basin, Australia; **(c), (d)**. Core cross section of stromatolite of the Fengcheng Fm., Well FC011, depth 3863.31–3863.73 m; **(e), (f)**. Chroococcus fossils from the 800-Ma-old Bitter Springs Fm. of central Australia; **(g)**. Chroococcus fossils from 1000-Ma-old Sukhaya Tunguska Fm. of Siberia, Russia; **(h)**. SEM photos of Chroococcus fossils from the Fengcheng Fm., Well FN1, 4253.5 m; **(i)**. Well F8, 3051.48 m, plane polarized light; **(j)**. Well F503, 3095.8 m, plane polarized light; **(k), (m)**. Kerogen maceral of the Fengcheng Fm., transmitted light, Well FN1, 4368.05 m; **(l), (n)**. Kerogen maceral of the Fengcheng Fm., UV light, Well FN1, 4368.05 m; **(o)**. Kerogen maceral of the Fengcheng Fm., transmitted light, Well FN1, 4423.05 m; **(p)**. Kerogen maceral of the Fengcheng Fm., UV light, Well FN1, 4423.05 m; **(q)**. Kerogen maceral of the Fengcheng Fm., transmitted light, Well FN1, 4124.96 m; **(r)**. Kerogen maceral of the Fengcheng Fm., UV light, Well FN1, 4124.96 m; In figures k–r, SA = sapropelic amorphogen; S = sporopollenite; HA = humic amorphogen; NV = normal vitrinite; F = fusinite. Scale bar in A is the decimeter ruler; The length of b is 33 cm; The red bars are scale bars in c–r; c & d = 1 cm; e–g = 10 μm; h & k–r = 50 μm; i & j = 20 μm; Pictures a, b, e–g, and i–j are from Awramik and Buchheim (2015), Coffey (2011), Schopf (2012), and Yu et al. (2021), respectively.

by the 2-methylhopane index (2-MHI, i.e., 2-methylhopanes/C_{30} 17, 21(H)-hopane) (Ding et al., 2020; Xia et al., 2021; Hou et al., 2022). A typical gas chromatogram at m/z 205 can be used to identify the 2-MHs with great accuracy (Summons et al., 1999; Peters et al., 2005; Hou et al., 2022). In this study, 2-MHs with carbon numbers between 28 and 36 (apart from 29) were found in samples from the Fengcheng Fm. (Fig. 5(e)). The 2α-methylhopane index (2-MHI) of the Fengcheng Fm. ranged from 3.91% to 23.14%, yielding an average of 9.89% (Table 1).

4.3.3. Steranes

Abundant regular steranes with carbon numbers of 27–29 were recognized in the m/z 217 mass chromatogram, with C_{29} steranes being the most abundant, followed by C_{28} steranes, and C_{27} steranes being the least abundant (Fig. 5f). The proportion of C_{29} steranes (C_{29}% = C_{29} steranes/sum (C_{27}–C_{29} steranes) × 100) ranges from 37.93% to 64.21%, with an average of 51.88% (Table 1).

5. Discussion

5.1. Significant contribution of cyanobacteria to OM of the Fengcheng Fm

5.1.1. Stromatolites, microbial fossils, and kerogen maceral analysis

Stromatolites, which are formed by cyanobacteria capturing mineral particles during their growth and metabolic processes,

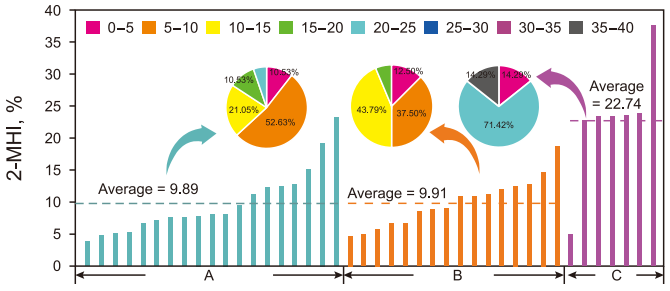

Fig. 9. 2-methylhopane index (2-MHI) of the Fengcheng Fm. **(a)**, the Precambrian sediments **(b)**, and the Tumbiana Fm. stromatolites **(c)** showing the high cyanobacteria input into the Fengcheng Fm. Data for the Precambrian sediments and the Tumbiana Fm. stromatolites are from Summons et al. (1999) and Coffey (2011), respectively.

serve as valuable indicators of cyanobacterial activity in sedimentary strata of alkaline lakes like the Green River Fm. (Fig. 8(a)) and the Tumbiana Fm. (Fig. 8(b)) (Coffey, 2011; Awramik and Buchheim, 2015). Laminated stromatolite was similarly observed in the cores of the Fengcheng Fm. (Fig. 8(c) and (d)). The identified part of the stromatolite was limited to its upper section, estimated to have a diameter exceeding 1.0 m. A distinct oval core with an irregular concentric shape was visible. These laminated stromatolites serve as compelling evidence of cyanobacteria's significant involvement in the deposition of the Fengcheng Fm. within the paleo-alkaline lake.

One of the oldest cyanobacterial species, Chroococcus sp., is readily recognized by its spheroidal cells covered in a thick sheath. Those microbial cells were commonly found in sediments that were deposited in the Precambrian period when cyanobacteria ruled the planet, for example in the 800 Ma-old Bitter Springs Fm. in central Australia, and the 1000 Ma-old Sukhaya Tunguska Fm. in Siberia, Russia (Schopf, 2012) (Fig. 8(a)–(c)). Similarly, many well-defined Chroococcus fossils were identified using SEM examination of the Fengcheng Fm. rocks (Fig. 8(d)). These fossils were about 10–30 μm in diameter, with relatively complete spherical or ellipsoidal structures. Some fossils exhibited a clear external outline and multi-cell structure (Fig. 8(d)). Yu et al. (2021) reported this kind of abundant spheroidal cyanobacteria in biogenic-induced chert layers from the Fengcheng Fm. as shown in Fig. 8(e) and (f). Those coccoid cyanobacteria are good indicators that help to illustrate the micropaleontological input to the Fengcheng Fm.

Kerogen maceral analysis is an economically efficient method that utilizes transmitted white light and reflected fluorescence to study the dispersed organic matter characteristics, origin, and optical parameters in source rocks (Tu et al., 2012; Omodeo-Salé et al., 2016). In this study, the sapropelinite group exclusively contains the maceral sapropelic amorphogen, while the maceral planktonic alginite is not present within this group (Fig. 8(k)–(r)). The amorphous bodies in the sapropelic amorphogen are typically flocculent or mist-like in appearance. They appear pale yellow to yellow-brown under transmitted light and exhibit bright yellow to brown fluorescence under UV light excitation (Fig. 8(k)–(r)). In the kerogen of the Fengcheng Fm., sapropelic amorphogen is the predominant maceral, constituting 70%–80%. Following that, fusinite is the next prominent maceral, accounting for 12%–19%. The remaining macerals include sporopollenite and humic amorphogen from the exinite group, normal vitrinite from the vitrinite group, and fusinite from the inertinite group, accounting for 8%–14% (Fig. 8(k)–(r)). Due to extensive degradation, the organic parent matrix cannot be identified for any biological structures after burial and diagenesis processes. While the main biological contributors for amorphous sapropel cannot be identified based on biological structures, previous studies on organic petrology analysis of cyanobacteria-rich sedimentary rocks and experimental simulations of cyanobacterial diagenesis have shown that cyanobacteria are prone to be degraded into sapropelic amorphogen after diagenesis (Cheng, 1997; Zhang and Xu, 2019). Base on a comprehensive analysis of stromatolites, microbial fossils, and kerogen maceral, we suggest that cyanobacteria are likely the major contributors to OM of the Fengcheng Fm. source rocks.

5.1.2. Lipid biomarker evidence

The Fengcheng Fm. has 2-MHI values ranging from 3.91% to 23.14%, with an average of 9.89% and 73% of all samples having values between 5% and 15% (Fig. 9(a)). Since cyanobacteria were the primary producers of OM prior to the Cambrian Explosion, particularly 1.5 billion years ago, it has been hypothesized that cyanobacteria are the main biological contributor to OM in the Precambrian strata (Glaessner and Foster, 1992; Wacey, 2013; Hou et al., 2022). The 2-MHI range of the Precambrian sediments is from 4.70% to 18.70%, with an average of 9.91%, and approximately 80% of samples have a range of 5%–15% (Fig. 9(b)), which suggests a 2-MHI level that is quite comparable to the Fengcheng Fm. The Tumbiana Fm. stromatolites were 2.7-Ga-old microbially induced sedimentary structures that formed in an ancient alkaline lake (Coffey, 2011), which were believed to be closely related to cyanobacteria's growth and metabolism (Huang et al., 2022; Yang et al.,

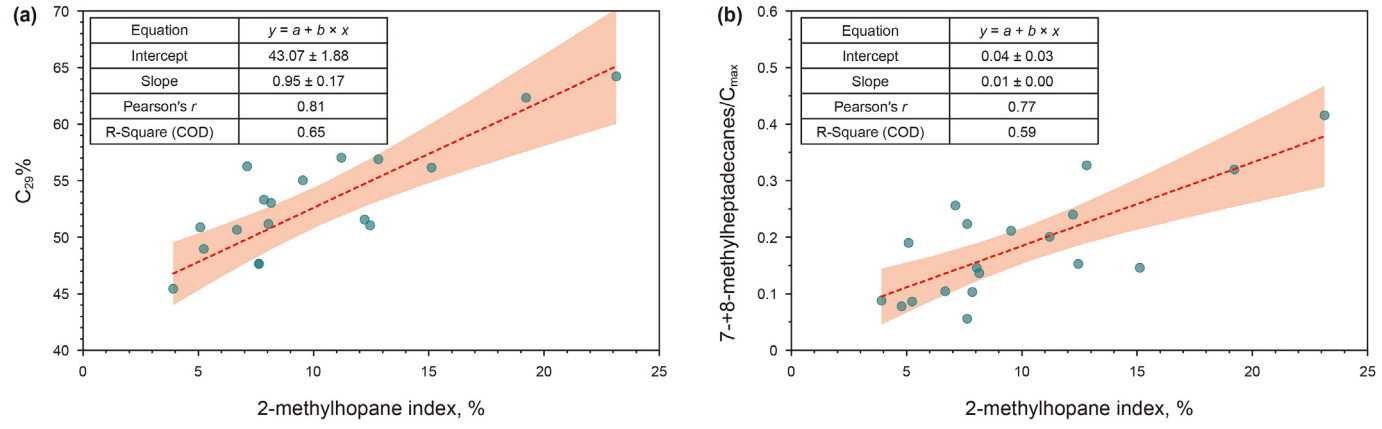

Fig. 10. The correlation between C_{29}%, 7- + 8-methyl heptadecanes/C_{max}, and 2-methylhopane index.

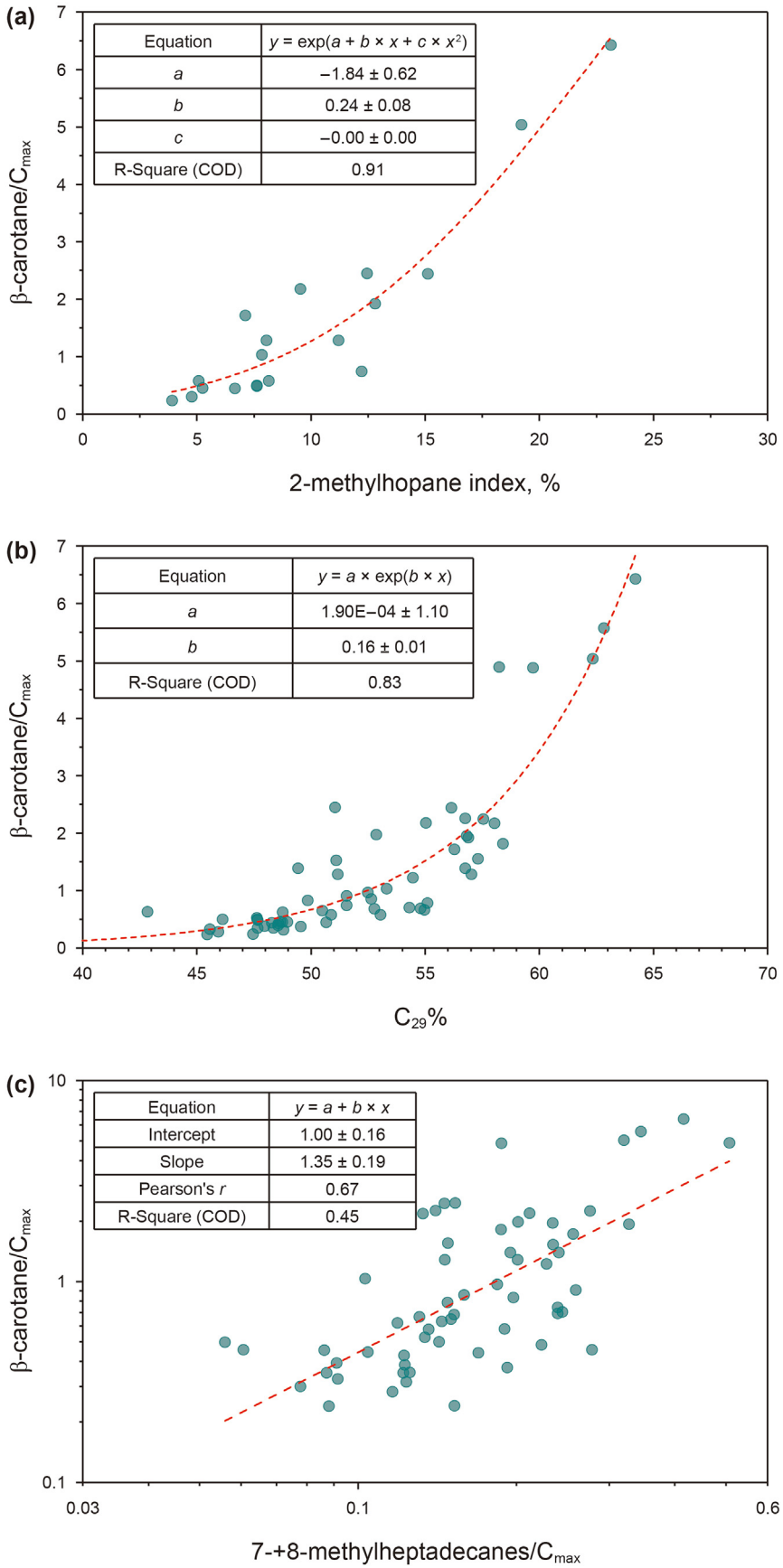

Fig. 11. The correlation between 2-methylhopane index, C_{29}%, 7- + 8-methyl heptadecanes/C_{max}, and β-carotane/C_{max} showing significant contribution of cyanobacteria to the enrichment of β-carotane of the Fengcheng Fm.

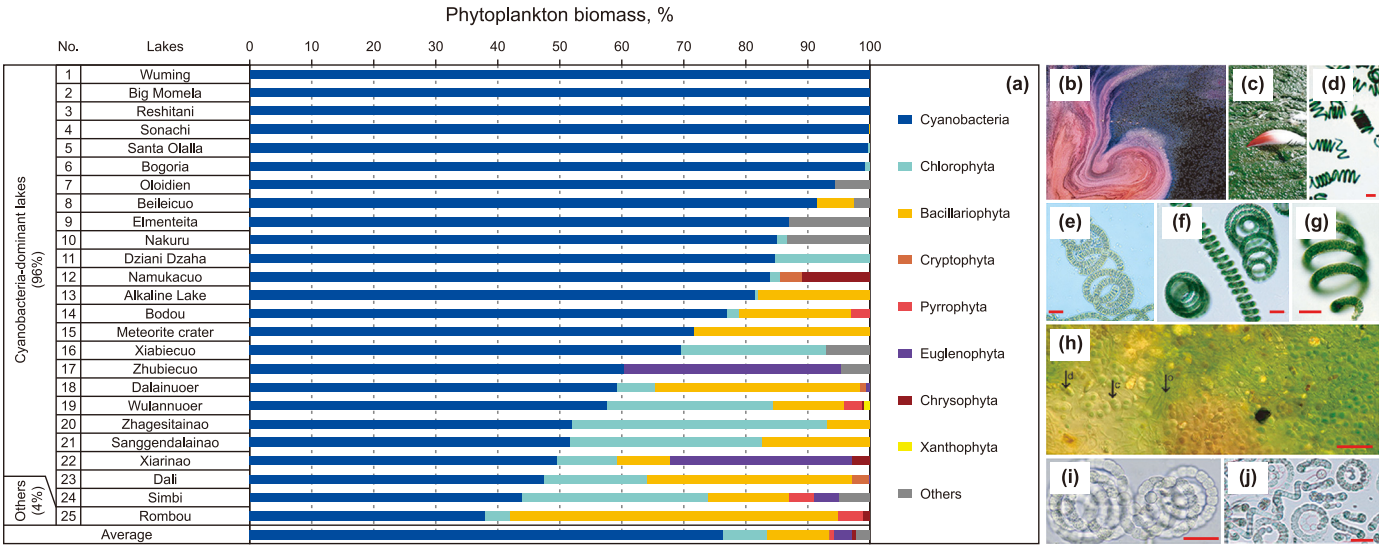

Fig. 12. Microbial community structure **(a)** and different species of cyanobacteria **(b)**–**(j)** in modern lakes. **(a)**. Data originate from Melack and Kilham (1974), Vareschi (1987), He et al. (1996), Wang and Dou (1998), López-Archilla et al. (2004), Ballot et al. (2005), Huo et al. (2005), Yang et al. (2008), Oberholster et al. (2009), Salm et al. (2009), Zhao (2010), Krienitz et al. (2013), and Yang (2014), Bernard et al. (2019), Opiyo (2020). **(b)**. Cyanobacteria mottled pattern on the lakesurface, Magadi lake, Kenya; **(c)**. Cyanobacteria mat, Oloidien lake, Kenya; **(d)**. Arthrospira maxima, Lake Texococo, Mexico; **(e)**. Spirulina platensis, Chagannor Lake, China; **(f)**. Arthrospira fusiformis, Kailala Lake, Chad; **(g)**. Arthrospira indica, Lake Lonar, India; **(h)**. Chroococcales (c), Oscillatoriales (o), and diatom (d) colonies in microbialite, Alchica Lake, Mexico; **(i)**. Cyanospira rippkae, Lake Nakuru, Kenya; **(j)**. Anabaenopsis elenkinii and Arthrospira, Lake Oloidien, Kenya. Pictures (**b**)–(**d**) and (**f**)–(**j**) are modified after Couradeau et al. (2011), Sili et al. (2012), Krienitz et al. (2013), Krienitz and Schagerl (2016), and Wu (2018); red bar markers = 20 μm.

2022). The Tumbiana Fm. stromatolites exhibit a 2-MHI range of 4.88%–37.55% with an average of 22.74% (Fig. 9(c)). Overall, the Tumbiana Fm. stromatolites possess larger 2-MHIs than those of the Fengcheng Fm. However, the pyrolysis action during the burial process plays a significant role in the transformation of 2-MHs from 2-methylhopanepolyols (Summons et al., 1999; Peters et al., 2005; Hou et al., 2022). Hou et al. (2022) explained that the lower 2-MHIs of the Fengcheng Fm. were ascribed to a delay in 2-MH transformation caused by the lower maturity of the Fengcheng Fm. over the Tumbiana Fm. The considerable abundance of 2-MHs in the Fengcheng Fm. suggests that cyanobacteria are the major source of OM, which is supported by comparisons with the Precambrian sediments and the Tumbiana Fm. stromatolites in 2-MHIs. This conclusion agrees with the finding that Hou et al. (2022) made after analyzing biomarkers, cyanobacteria fossils, and stromatolites.

One of the remarkable features of the Fengcheng Fm. is the high abundance of the C_{29} steranes over the C_{27} and C_{28} steranes (Fig. 5(f)). Previous investigations had generated controversy that C_{29} steranes are typically derived from land plants (Huang and Meinschein, 1979; Ding et al., 2017), algae (Xia et al., 2022), and cyanobacteria (Hou et al., 2022). With a correlation coefficient of 0.81, the 2-MHI and C_{29}% correlation demonstrates a very strong positive link between them (Fig. 10(a)). A similar positive association between these two parameters can be found in the Tumbiana Fm. (Hou et al., 2022). It implies that cyanobacteria are a significant biological source for the C_{29} steranes in the Fengcheng Fm. Hence, the high abundance of the C_{29} steranes actually typifies a major contribution of cyanobacteria to the OM of the Fengcheng Fm.

High concentrations of 7- + 8-MHs in modern cyanobacteria, cyanobacteria-rich sediments, and numerous Precambrian sediments and oil appear to suggest an origin from cyanobacteria (Peters et al., 2005). The 7- + 8-MHs/C_{max} ratio was frequently used to evaluate cyanobacteria's contribution to OM in sediments and oils (Summons et al., 1999; Ding et al., 2020; Xia et al., 2021, 2022). In this study, the 7- + 8-MHs/C_{max} ratio of the Fengcheng Fm. exhibits a positive correlation with 2-MHI, with a correlation coefficient of 0.77 (Fig. 10(b)). Abundant 7- + 8-MHs in the Fengcheng Fm. likewise originate from cyanobacteria.

In summary, cyanobacteria are therefore identified as the major producers of the OM of the Fengcheng Fm. source rocks based on a comprehensive analysis of biomarkers such as 2-MHI, C_{29}%, and 7- + 8-MHs, as well as cyanobacteria fossils found in petrographic thin sections and SEM.

5.2. Cyanobacteria's contribution to biological precursor of β-carotane

β-carotane, a fully saturated lipid (see Fig. 5(b)), is converted from β-carotene with a C_{40} carotenoid structure in a reductive hydrogenation reaction (Ding et al., 2017; Ogbesejana et al., 2022).

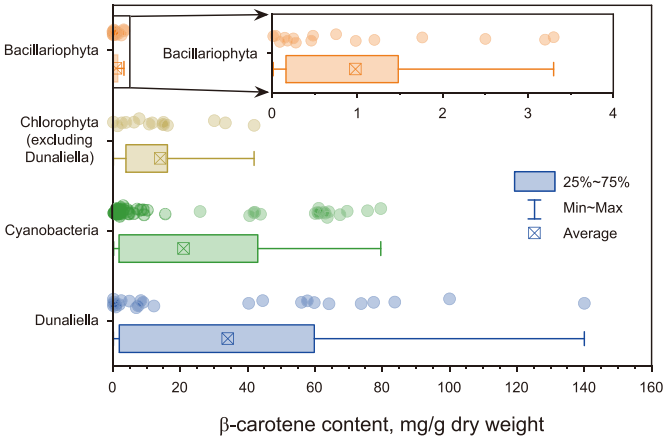

Fig. 13. The β-carotene content of three primary phytoplankton populations in modern alkaline lakes. Data are from Pennington et al. (1988), Gómez-Pinchetti et al. (1992), Liu et al. (1995), Jiang and Yao (1997), Yuan et al. (1997), Guo et al. (1999), Pick (2002), Kang et al. (2006), Fang, 2012, Wu et al. (2013), and Patias et al. (2017), Tran et al. (2019), and Diao et al. (2020).

Therefore, a considerable biological precursor supplement of β-carotene is necessary for the enrichment of β-carotane. β-carotene can theoretically originate from higher plants, algae, and photosynthetic bacteria (Black, 2004; Brocks and Schaeffer, 2008). Lipid biomarkers and biochemical analyses were comprehensively used to unravel the biological precursor of β-carotane in the Fengcheng Fm.

5.2.1. Lipid biomarker evidence

As mentioned above, high concentrations of 2-MHs, C_{29} steranes, and 7- + 8-MHs are effectively indicative of cyanobacterial blooms. 2-MHI and C_{29}% demonstrate a potent exponential correlation with the β-carotane index, with R^2 values of 0.91 and 0.83, respectively (Fig. 11(a) and (b)). The abundance of 7- + 8-MHs is notably higher than that of other branched homologs (Fig. 5). A positive correlation between 7- + 8-MHs/C_{max} and the β-carotane index was observed, with a correlation coefficient of 0.67 (Fig. 11c). Some samples possess β-carotane indexes greater than 4, which is a response to significant cyanobacterial input, as shown by high 2-MHI, C_{29}%, and 7- + 8-MHI. As a result, the significant positive correlation between the three cyanobacteria indicators and the β-carotane index suggests that cyanobacteria are the primary biological contributors of β-carotane.

5.2.2. The dominant phytoplankton and their β-carotene content in modern alkaline lakes

The principle of "uniformitarianism", stating that the present is the key to the past, was frequently utilized by many geologists to reconstruct ecosystems, tectonic geology, and sedimentology (Windley, 1993; Johnson, 2014). By researching the microbial community structures and the β-carotene content of the dominant phytoplankton in modern alkaline lakes, we attempted to shed light on the biological precursors of β-carotane in the Fengcheng Fm.

The biomass of phytoplankton in 25 alkaline lakes was statistically analyzed. The findings demonstrate the overwhelming predominance of cyanobacteria over other algal species in these alkaline lakes, and the proportion of cyanobacteria-rich lakes is up to 96% (Fig. 12(a)). The cyanobacteria biomass makes up 44%–100% of the cyanobacteria-rich lakes. Modern alkaline lakes (e.g., lakes 1–13) are often monospecific and inhabited by cyanobacteria, with cyanobacteria's biomass exceeding 80%. Cyanobacteria, Chlorophyta (green algae), and Bacillariophyta (diatoms) have average biomasses of 76.40%, 7.06%, and 10.00%, respectively (Fig. 12(a)). Cyanobacteria account for the vast majority of biomass, followed by diatoms and green algae. Different species of cyanobacteria, such as Arthrospira maxima, Spirulina platensis, Arthrospira fusiformis, and Arthrospira indica, etc., were discovered in modern alkaline lakes, as shown in Fig. 12(b)–(j).

Although the high salinity and alkalinity of alkaline lakes are extremely hostile to most aquatic organisms' survival, cyanobacteria can outcompete them to be the dominant phytoplankton (Grant, 2006). It can be attributed to the following reasons: (i) cyanobacteria possess an excellent capacity to synthesize abundant antioxidants such as carotenoids and vitamin E by utilizing sufficient sodium in alkaline waters to avoid oxidative damage caused by saline and alkaline stress (Alsenani et al., 2020; Almendinger et al., 2021); (ii) cyanobacteria can fully utilize inorganic carbon sources from alkaline waters to photosynthesize by an inorganic carbon-concentrating mechanism (Klanchui et al., 2017; Katayama, 2022); and (iii) the highly saline and alkaline stress of alkaline waters are unfavorable habitats for some species of algae (Newsted, 2004; Hwang et al., 2006; Wu, 2012; Zheng, 2015). The highly alkaline waters appear to hinder the growth of some species of Chlorophyta, Phaeophyta, and Bacillariophyta (Newsted, 2004; Hwang et al., 2006; Wu, 2012; Zheng, 2015). In modern alkaline lakes (e.g., Lakes No. 19–21, 24) with relatively abundant Chlorophyta, the primary species of Chlorophyta are Chlorellla vulgaris, Pediastum boryanum, Oocystis sp., Crucigenia sp., Cosmarium sp., etc. rather than Dunaliella (Huo et al., 2005; Yang et al., 2008; Opiyo, 2020). Dunaliella, a well-known species of halotolerant algae, is unexpectedly rare in modern alkaline lakes. However, Dunaliella (especially Dunaliella salina) has been recognized as the predominant species in modern chloride lakes such as the Urmia Lake in Iran, the Great Salt Lake in the USA (Marcarelli et al., 2006), and the Lake Krasnovishnevoye in Russia (Komova et al., 2018). Chloride lakes commonly have a higher salt concentration than those of carbonate lakes (i.e., alkaline lakes) (Schagerl and Renaut, 2016). Dunaliella appears to be more resistant to higher salinity stress, but is seemingly unable to tolerate highly alkaline environments and thus loses its advantage of outcompeting cyanobacteria in alkaline lakes.

Further, the β-carotene content of three primary phytoplankton populations (i.e., Cyanobacteria, Chlorophyta, and Bacillariophyta) in modern alkaline lakes was biochemically analyzed to verify potential biological sources of β-carotene. The results demonstrate that Bacillariophyta yields the least β-carotene with a minimum, maximum, and average of 0.02, 3.20, and 0.62 mg/g dry weight, respectively. Chlorophyta (excluding Dunaliella) produce a fair amount of β-carotene ranging from 0.09 to 16.21 mg/g dry weight, with an average of 5.94 mg/g dry weight (Fig. 13). The β-carotene content of cyanobacteria exhibits a range of 0.2–79.56 mg/g dry weight, with an average of 20.97 mg/g dry weight. This suggests that cyanobacteria have a lower abundance of β-carotene compared to Dunaliella, known for being an excellent source with β-carotene content ranging from 1.90 to 140 mg/g dry weight and an average of 39.24 mg/g dry weight. As a result, in terms of biomass and β-carotene content, cyanobacteria are the ideal biological source of β-carotene in alkaline lakes.

5.3. Environmental factors of β-carotane enrichment

The alkaline lake depositional characteristics of the Fengcheng Fm. were well recognized by previous investigators (Zhang et al., 2018; Yu et al., 2019; Xia et al., 2021, 2022; Hou et al., 2022). According to the characteristics of paleoclimate, paleoredox, and paleosalinity, the ancient alkaline lake evolution process of the Fengcheng Fm. can be divided into three stages, i.e., the early (A), primary (B), and late (C) stages (Fig. 14). The β-carotane enrichment affected by environmental factors was investigated by making correlations between depositional environmental factors and β-carotane.

5.3.1. Paleoclimate

Alkaline lakes around the world, mostly located in tropic and subtropical areas (Hou et al., 2022), are characterized by closed, warm, arid, and heavily evaporative environments (Melack and MacIntyre, 2016; Lowenstein et al., 2017; Yu et al., 2019). Alkaline minerals such as shortite, northupite, wegscheiderite, nahcolite, trona, and sodium carbonate were frequently discovered in sediments of ancient and modern alkaline lakes, such as the Observation Hill Fm. in Australia (White and Youngs, 1980), the Green River Fm. in the United States (Lowenstein et al., 2017), the Mülk Fm. (Helvaci, 2019) in Turkey, the Hetaoyuan Fm. in China (Li et al.,

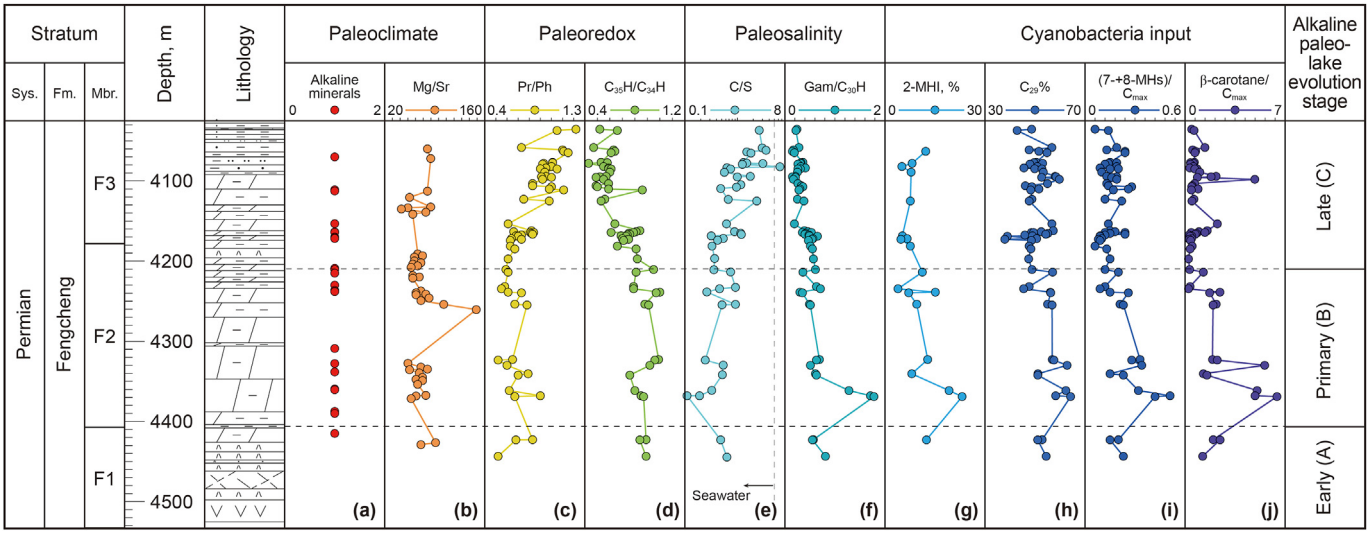

Fig. 14. The typical geochemical profile of the Fengcheng Fm. showing the paleoclimate, paleoredox, paleosalinity, and cyanobacteria input of the three evolution stages of the Fengcheng ancient alkaline lake. The legend for lithological is the same as that in Fig. 1(e). Data for Mg/Sr are from Zhang et al. (2018). The lithology legend is identical to that in Fig. 1.

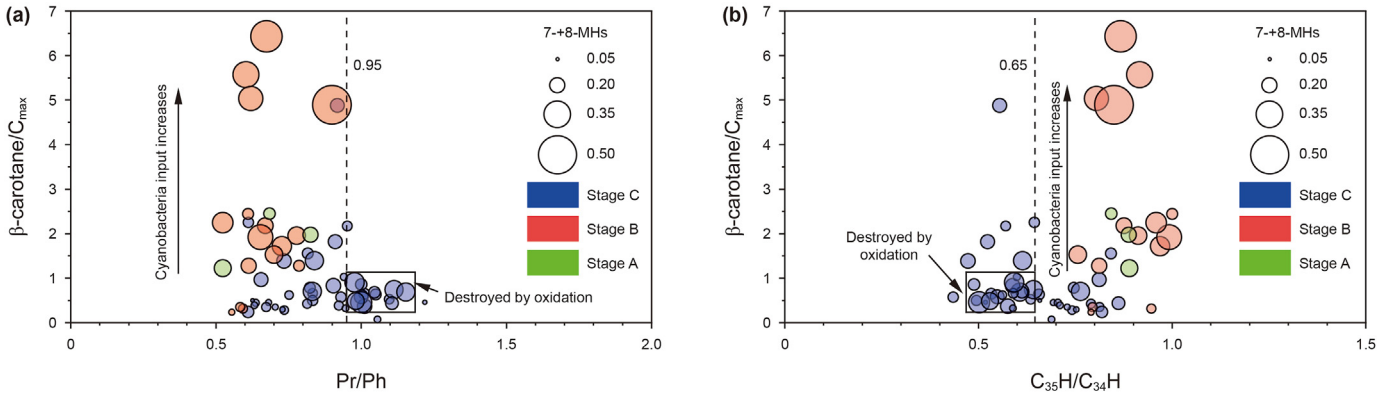

Fig. 15. Scatter-plots of pristane/phytane (Pr/Ph), C_{35} homohopanes (22 S + 22 R)/C_{34} homohopanes (22 S + 22 R) ($C_{35}H/C_{34}H$) versus β-carotane/C_{max} of samples with different 7- + 8- methyl heptadecanes/C_{max} showing the relation between the paleoredox condition and the enrichment of β-carotane in the Fengcheng Fm.

2017), and the Magadi Lake in Kenya (Lowenstein et al., 2017). Saline lake geologists suggested that these alkaline minerals formed in xerothermic environments with temperatures above 15 °C and little precipitation (Friedman et al., 1976; Zheng et al., 1998). The Fengcheng Fm. also contained large amounts of alkaline minerals (Fig. 14(a)), implying that it was deposited in an xerothermic environment. It was found that the distribution coefficient of Mg is positively correlated with water temperature, while that of Sr shows little or no correlation to temperature (Gascoyne, 1983). Therefore, the Mg/Sr ratio has been used as a tool for paleoclimate characterization, and the larger ratios indicate a more xerothermic climate (Gascoyne, 1983). In stages A, B, and C of the Fengcheng alkaline paleo-lake evolution, the Mg/Sr ratio varies from small, large, and medium levels (Fig. 14(b)), indicating weakly, heavily, and farily xerothermic climates, respectively, which matches well with the results reflected by the alkaline minerals' number in every stage. The paleoclimate appears to be weakly correlated to β-carotane/C_{max} which shows medium, large, and small values in stages A, B, and C, respectively (Fig. 14(j)). It suggests that the paleoclimate condition does not significantly affect the enrichment of β-carotane in the Fengcheng Fm., but has some influence on the paleosalinity of lake water by controlling evaporation and precipitation.

5.3.2. *Paleoredox*

The Pr/Ph and $C_{35}H/C_{34}H$ ratios were used to effectively indicate the paleoredox condition (Peters et al., 2005; Ding et al., 2017; Hou et al., 2022). The results show a good negative correlation between Pr/Ph and $C_{35}H/C_{34}H$ in the Fengcheng Fm. (Fig. 14(c) and (d)). The majority of samples have Pr/Ph values of under 1.0, and $C_{35}H/C_{34}H$ values of over 0.65, implying that the Fengcheng Fm. was deposited in the reducing water. In the early and primary alkaline lake evolution stages, the depositional water is typically strongly reducing, while it turns out to be weakly reducing or weakly oxidizing in the late stage (Fig. 14(c) and (d)). β-carotene is readily destroyed by oxidation, consequently, its reduced product 'β-carotane' in sediment was commonly used to typify a reducing depositional

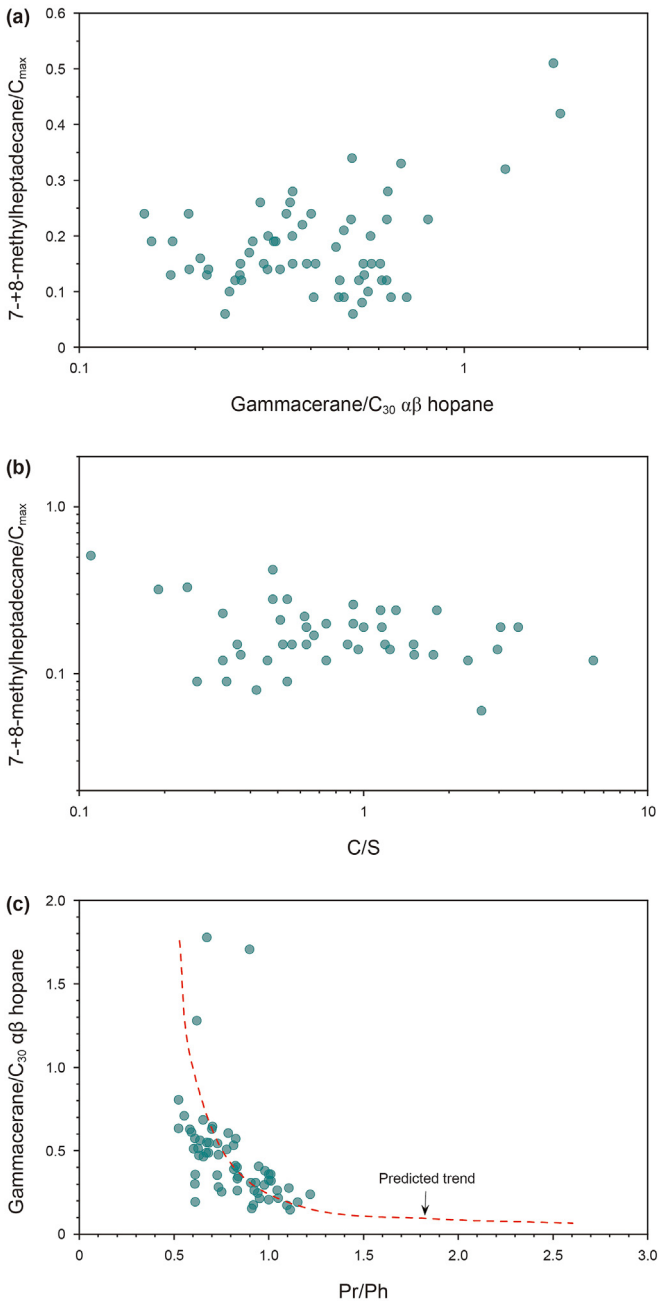

Fig. 16. Scatter-plots of gammacerane/C_{30} αβ hopane versus 2-methylhopane index and pristane/phytane (Pr/Ph) versus gammacerane/C_{30} αβ hopane showing the relationships between cyanobacteria input, the paleoredox condition, and the paleosalinity, respectively.

environment (Peters et al., 2005; Ding et al., 2017). The abundance of β-carotane unexpectedly shows weak correlations with two paleoredox proxies (Fig. 15(a) and (b)). This is attributed to the reality that the Fengcheng Fm. was mainly deposited in a reductive environment, thus the redox condition does not significantly affect the enrichment of β-carotane. Instead, the abundance variation of β-carotane is more likely linked to its biological precursor content. There appears to be a certain threshold for redox conditions that start to affect the enrichment of β-carotane. In this study, the thresholds of Pr/Ph and $C_{35}H/C_{34}H$ are 0.95 and 0.65, respectively. When Pr/Ph values are under 0.95 and $C_{35}H/C_{34}H$ values are over 0.65, the β-carotane abundance is positive with cyanobacteria input indicated by 7- + 8-MHs (Fig. 15(a) and (b)), which means that the low values of β-carotane/C_{max} are caused by less cyanobacteria input. While some samples (in the black rectangle of Fig. 15(a) and (b)) maintain substantial cyanobacterial input at Pr/Ph ratios over 0.95 and $C_{35}H/C_{34}H$ values under 0.65, their β-carotane abundance appears abnormally low, which is related to the loss of β-carotene induced by oxidation processes.

5.3.3. Paleosalinity

Organic carbon/sulfur ratio (C/S) is a useful water salinity proxy, and its thresholds for freshwater, brackish, and seawater are > 10, 5–10, and < 5, respectively (Berner and Raiswell, 1984; Wei et al., 2018). The C/S ratio of the Fengcheng Fm. ranges from 0.11 to 6.44, with an average of 1.12. All samples from stages A and B possess C/S ratios of < 1, while samples from stage C are relatively larger, but most of them are < 5 (Fig. 14(e)), indicating the hypersaline and saline-to-hypersaline characteristics in the evolution stages A, B, and C of the Fengcheng Fm., respectively. High salinity is a significant factor in promoting water column stratification (Ding et al., 2017; Ma and Cui, 2022; Xia et al., 2022). We suggest a large gammacerane index is caused by the high salinity of the Fencheng Fm., and the gammacerane index is a response to the Fencheng Fm.'s salinity. The gammacerane index exhibits a positive correlation with β-carotane/C_{max} (Fig. 14f–j), which implies that the paleosalinity affects the β-carotane enrichment to a certain degree. The high β-carotane index was also frequently reported to typify saline or hypersaline environments (Mello et al., 1993; Tao et al., 2019). Nevertheless, the enrichment of β-carotane is closely related to a sufficient precursor supply, a reducing condition, and well preservation (Ding et al., 2017, 2020; Wang et al., 2022). Theoretically, the enrichment of β-carotane does not require a high salinity condition. However, it was discovered that 7- + 8-MHs/C_{max} has a weak positive and negative correlation with the gammacerane index, respectively (Fig. 16(a) and (b)), implying that salinity somehow influences cyanobacteria input. Moreover, Pr/Ph negatively correlates with the gammacerane index (Fig. 16(c)), as previous investigations reported (Ding et al., 2017; Ma and Cui, 2022), suggesting that strong water column stratification brought on by high salinity favors a reducing condition. As a result, high paleosalinity is not a direct factor in controlling the β-carotane enrichment, but it can improve precursor supply from cyanobacteria and provide an advantageous reducing condition, which indirectly favors the β-carotane enrichment in the Fengcheng Fm.

5.4. Enrichment model of β-carotane

Based on comprehensive analyses of the influence factors of β-carotane enrichment and the evolution process of the Fengcheng ancient alkaline lake, a β-carotane enrichment model controlled by the coupling of volcanism, biological precursor, and depositional environment was established (Fig. 17).

Most modern alkaline lakes worldwide are discovered in volcanic terrain, and their development is linked to volcanic events (Grant, 2006; Pecoraino et al., 2015; Schagerl and Renaut, 2016). Volcanism vitally contributes to the hydrochemistry and biological evolution of alkaline lakes (Pecoraino et al., 2015; Schagerl and Renaut, 2016). Excess CO_2 from volcanism dissolved in the water and accelerated the chemical weathering of volcanic bedrock, yielding abundant K^+, Na^+, and HCO_3^- (Earman et al., 2005; Pecoraino et al., 2015), which provided dominant ions to enable the hydrochemical evolution of alkaline lakes. In addition, inorganic

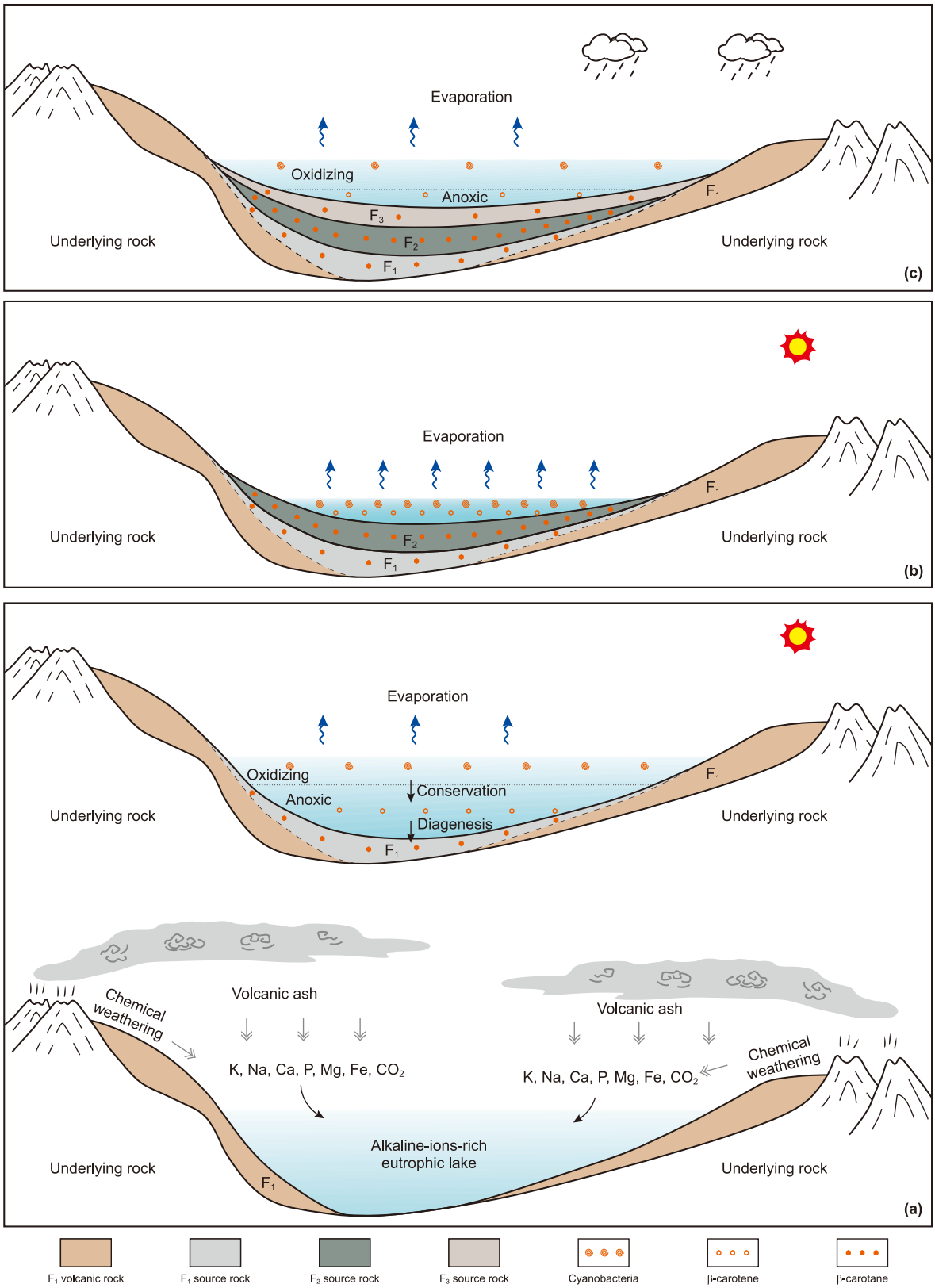

Fig. 17. The enrichment model of β-carotane in the Early (**a**), Primary (**b**), and Late (**c**) evolution stages of the Fengcheng alkaline paleo-lake.

nutrient elements such as nitrogen, phosphorus, potassium, iron, and calcium from volcanic ash and debris fell or flowed into the lake, facilitating the lake's eutrophia and inducing the bloom of aquatic phytoplankton such as cyanobacteria and algae (Lin et al., 2011; Schagerl and Renaut, 2016). It was previously investigated that volcanic events were prevalent during the early stage of the Fengcheng Fm. (Zhang et al., 2018). Consequently, volcanic rocks such as andesite, tuff, and rhyolite formed on the bottom of the Fengcheng Fm. (Fig. 1(e)). Volcano eruptions and chemical weathering of volcanic bedrocks in the early stage of the Fengcheng Fm. provided chemical solutes for the evolution of the Fengcheng alkaline paleo-lake and rich nutrients for phytoplankton blooms in the Fengcheng alkaline paleo-lake's early evolution stage (Fig. 17(a)).

After volcanic eruptions, the ancient alkaline lake evolved in the development stage. The climate became xerothermic, accelerating lake water evaporation and concentration, resulting in high salinity and alkalinity during this stage (Fig. 17(a)). This special water condition with high salinity and alkalinity plays a crucial role in the enrichment of β-carotane in the Fenghcheng Fm. in two aspects. Firstly, most creatures cannot survive in this hostile environment with high salinity and alkalinity. Nonetheless, haloalkaliphilic cyanobacteria, as extremophiles with strong vitality, possess an overwhelming advantage in adapting to and thriving in this alkaline lake (Fig. 14(g)–(i)). Cyanobacteria's large biomass and high β-carotene content provide significant biological precursors for β-carotane. Secondly, the high salinity and alkalinity of the Fengcheng paleolake facilitates water column stratification, which yields an anoxic zone at the bottom. The anoxic condition favored β-carotene to avoid oxidative damage and to be transformed into β-carotane by diagenesis in a hydrogenation reduction reaction. Thus, a certain amount β-carotane was produced after the conservation and diagenesis of β-carotene in the Lower Member of the Fengcheng Fm. (F_1).

In the primary evolution stage (b) of the Fengcheng alkaline paleolake, the climate became more xerothermic, leading to a faster evaporation and concentration of lake water and a higher salinity and alkalinity of the water column. A higher salinity and alkalinity condition boosts the predominance of cyanobacteria and the reducing condition of lake water. Hence, the most abundant β-carotane was synthesized in the primary evolution stage (b) of the Fengcheng alkaline paleolake (Fig. 14(j)) due to a substantial β-carotene supply and a favorable reducing environment (Fig. 17(b)).

In the late evolution stage (c) of the Fengcheng paleolake, the climate got relatively humid and the precipitation increased. As a result of reduced evaporation and freshwater supply, the water depth of the paleolake increased while its salinity and alkalinity decreased. The overwhelming advantages of cyanobacteria over other phytoplankton were weakened, and the cyanobacteria input was consequently reduced, thus decreasing the biological precursor of β-carotane. In addition, the water column was not significantly stratified due to the decrease in salinity, which led to a relatively weak reduction of bottom water. Therefore, the β-carotane abundance is relatively lower in the late evolution stage (c) than that of the primary evolution stage (b) of the Fengcheng alkaline paleolake (Fig. 17(c)).

6. Conclusions

The source rocks in the Fengcheng Fm. possess high TOC and $S_1 + S_2$ values, medium H/C ratios, indicating that they are good source rocks with a high abundance of OM and a significant potential of oil and gas generation. Cyanobacteria are supposed to be primary contributors to the Fengcheng Fm.'s OM based on a comprehensive investigation of cyanobacteria fossils, biomarkers (high abundances of 2-MHs, 7- + 8-MHs, and C_{29}%), and the dominance of cyanobacteria in modern alkaline lakes. The Fengcheng Fm. was deposited in an xerothermic, reducing, saline-hypersaline environment that is indicated by abundant alkaline minerals, large Mg/Sr, low Pr/Ph, high $C_{35}H/C_{34}H$, a high gammacerane index, and a low C/S atomic ratio, respectively.

Abundant β-carotane is, above all, an indicator of biological input to OM in sediments. Based on molecular geochemical analysis of cores and biochemical analysis of modern alkaline lakes, we suggest that the haloalkaliphilic cyanobacteria with abundant β-carotene are the primary biological sources to supply the precursor of β-carotane. The cyanobacteria input contribution is the decisive factor for the enrichment of β-carotane in the Fengcheng Fm.

The paleoclimate condition does not significantly affect the enrichment of β-carotane in the Fengcheng Fm., but somehow impacts the water's paleosalinity by affecting evaporation and precipitation. The Fengcheng Fm.'s abundance of β-carotane does not exhibit a clear association with the paleoredox condition because it was mostly deposited in a reducing environment. But the β-carotane abundance is indeed relatively low due to the oxidative damage under a weakly reducing condition in the late evolution stage of the Fengcheng paleolake. The hypersaline condition is not a direct and necessary factor to affect the enrichment of β-carotane. Nevertheless, the hypersaline condition improves the precursor supply from cyanobacteria and creates an advantageous reducing condition, which indirectly favors the enrichment of β-carotane in the Fengcheng Fm.

Declaration of interest statement

We confirm that this manuscript has not been published elsewhere and is not under consideration by another journal. All authors have approved the manuscript and agreed with its submission to Petroleum Science. There is no conflict of interest to declare.

Acknowledgements

We thank the financial support from the National Key Research and Development Program of China (2019YFC0605502), the National Natural Science Foundation of China (42302156), the Major Projects of PetroChina Science and Technology Fund (2021DJ0206), and the Natural Science Foundation of China University of Petroleum (22CX06046A). We are appreciative of the core samples' donation from the Xinjiang Petroleum Administration Bureau of CNPC.

Appendix A. Supplementary data

Supplementary data to this article can be found online at https://doi.org/10.1016/j.petsci.2023.12.019.

References

Almendinger, M., Saalfrank, F., Rohn, S., Kurth, E., Springer, M., Pleissner, D., 2021. Characterization of selected microalgae and cyanobacteria as sources of compounds with antioxidant capacity. Algal Res. 53, 102168. https://doi.org/10.1016/j.algal.2020.102168.

Alsenani, F., Tupally, K.R., Chua, E.T., Eltanahy, E., Alsufyani, H., Parekh, H.S., Schenk, P.M., 2020. Evaluation of microalgae and cyanobacteria as potential sources of antimicrobial compounds. Saudi Pharmaceut. J. 28 (12), 1834–1841. https://doi.org/10.1016/j.jsps.2020.11.010.

Awramik, S.M., Buchheim, H.P., 2015. Giant stromatolites of the Eocene Green River formation (Colorado), USA. Geology 43 (8), 691–694. https://doi.org/10.1130/G36793.1.

Ballot, A., Krienitz, L., Kotut, K., Wiegand, C., Pflugmacher, S., 2005. Cyanobacteria and cyanobacterial toxins in the alkaline crater lakes Sonachi and Simbi, Kenya. Harmful Algae 4 (1), 139–150. https://doi.org/10.1016/j.hal.2004.01.001.

Bernard, C., Escalas, A., Villeriot, N., Agogué, H., Hugoni, M., Duval, C., Carré, C., Got, P., Sarazin, G., Jézéquel, D., Leboulanger, C., Grossi, V., Ader, M., Troussellier, M., 2019. Very low phytoplankton diversity in a tropical saline-alkaline lake, with Co-dominance of Arthrospira fusiformis (cyanobacteria) and Picocystis salinarum (Chlorophyta). Microb. Ecol. 78 (3), 603–617. https://doi.org/10.1007/s00248-019-01332-8.

Berner, R.A., Raiswell, R., 1984. C/S method for distinguishing freshwater from marine sedimentary rocks. Geology 12 (6), 365–368. https://doi.org/10.1130/0091-7613(1984)12<365:cmfdff>2.0.co;2.

Black, H.S., 2004. Pro-carcinogenic activity of β-carotene, a putative systemic photoprotectant. Photochem. Photobiol. Sci. 3 (8), 753–758. https://doi.org/10.1039/b316438a.

Brocks, J.J., Schaeffer, P., 2008. Okenane, a biomarker for purple sulfur bacteria (Chromatiaceae), and other new carotenoid derivatives from the 1640 Ma Barney Creek Formation. Geochem. Cosmochim. Acta 72 (5), 1396–1414. https://doi.org/10.1016/j.gca.2007.12.006.

Chen, Z.L., Liu, G.D., Wei, Y.Z., Gao, G., Ren, J.L., Yang, F., Ma, W.Y., 2017. Distribution pattern of tricyclic terpanes and its influencing factors in the Permian source rocks from Mahu Depression in the Junggar Basin. Oil Gas Geol. 38 (2), 311–322 (in Chinese).

Cheng, D.S., 1997. Macerals and petrology of palaeozoic source rock in Tarim basin. Xinjing Pet. Geol. 18 (1), 40–45 (in Chinese).

Coffey, J.M., 2011. A Paleoenvironmental Study of the 2.7 GA Tumbiana Formation, Fortescue Basin, Western Australia. PhD thesis, University of New South Wales, Sydney, pp. 1–296.

Couradeau, E., Benzerara, K., Moreira, D., Gérard, E., Kaźmierczak, J., Tavera, R., López-García, P., 2011. Prokaryotic and Eukaryotic community structure in field and cultured microbialites from the alkaline lake Alchichica (Mexico). PLoS One 6, e28767. https://doi.org/10.1371/journal.pone.0028767.

Diao, J.J., Song, X.Y., Zhang, L., Cui, J.Y., Chen, L., Zhang, W.W., 2020. Tailoring cyanobacteria as a new platform for highly efficient synthesis of astaxanthin. Metab. Eng. 61, 275–287. https://doi.org/10.1016/j.ymben.2020.07.003.

Ding, W.J., Hou, D.J., Jiang, L., Jiang, Y.H., Wu, P., 2020. High abundance of carotanes in the brackish-saline lacustrine sediments: a possible cyanobacteria source? Int. J. Coal Geol. 219, 103373. https://doi.org/10.1016/j.coal.2019.103373.

Ding, X.J., Gao, C.H., Zha, M., Chen, H., Su, Y., 2017. Depositional environment and factors controlling β-carotane accumulation: a case study from the Jimsar Sag, Junggar Basin, northwestern China. Palaeogeogr. Palaeoclimatol. Palaeoecol. 485, 833–842. https://doi.org/10.1016/j.palaeo.2017.07.040.

Earman, S., Phillips, F.M., McPherson, B.J.O.L., 2005. The role of "excess" CO_2 in the formation of trona deposits. Appl. Geochem. 20 (12), 2217–2232. https://doi.org/10.1016/j.apgeochem.2005.08.007.

Fang, M., 2012. Extraction and Hypoglycemic Effect of Beta-Carotene from Spirulina Platensis. Beijing Forestry University (in Chinese).

Friedman, I., Smith, G.I., Hardcastle, K.G., 1976. Studies of quaternary saline lakes—II. Isotopic and compositional changes during desiccation of the brines in Owens Lake, California, 1969–1971. Geochem. Cosmochim. Acta 40 (5), 501–511. https://doi.org/10.1016/0016-7037(76)90218-0.

Gascoyne, M., 1983. Trace-element partition coefficients in the calcite-water system and their paleoclimatic significance in cave studies. J. Hydrol. 61 (1–3), 213–222. https://doi.org/10.1016/0022-1694(83)90249-4.

General Administration of Quality Supervision, Inspection and Quarantine, 2010. Isolation Method for Kerogen from Sedimentary Rock: GB/T19144-2010. Standards Press of China, Beijing.

Glaessner, M.F., Foster, C.B., 1992. Paleontology and biogeochemical research: a powerful synergy. In: Schidlowski, M., Golubic, S., Kimberley, et al. (Eds.), Early Organic Evolution. Springer, Berlin, Heidelberg. https://doi.org/10.1007/978-3-642-76884-2_13.

Gómez-Pinchetti, J.L., Ramazanov, Z., Fontes, A., García-Reina, G., 1992. Photosynthetic characteristics of Dunaliella salina (Chlorophyceae, Dunaliellales) in relation to β-carotene content. J. Appl. Phycol. 4 (1), 11–15. https://doi.org/10.1007/bf00003955.

Grant, W.D., 2006. Alkaline environments and biodiversity. In: Gerday, C., Glansdorff, N. (Eds.), Extremophiles, vol. III. Eolss Publishers, Oxford, pp. 21–38.

Grba, N., Šajnović, A., Stojanović, K., Simić, V., Jovančićević, B., Roglić, G., Erić, V., 2014. Preservation of diagenetic products of β-carotene in sedimentary rocks from the Lopare Basin (Bosnia and Herzegovina). Geochemistry 74 (1), 107–123. https://doi.org/10.1016/j.chemer.2013.10.002.

Gu, Y.L., 2021. Determination of Oil Sources in the Western Slope of Mahu Sag, Junggar Basin on the Basis of Compound Specific Carbon Isotopes and Molecular Parameters and Concentrations. Master Dissertation of University of Chinese Academy of Sciences (in Chinese).

Guo, H.B., Zhong, J.J., Su, Z.R., 1999. The content measurement of beta-carotene in Spirulina platensis. J. Biol. 16 (4), 31–32 (in Chinese).

He, Z.H., Jiang, H., Bi, F.S., 1996. Restudies on the hydrochemistry and hydrobiology of Dali lake. J. Dal. Fish. College. 11 (2), 1–13 (in Chinese).

Helvaci, C., 2019. Turkish trona deposits: geological setting, genesis and overview of the deposits. In: Pirajno, F., Ünlü, T., Donmez, ¨ C., S¸ahin, M. (Eds.), Mineral Resources of Turkey, Modern Approaches in Solid Earth Sciences, vol. 16. Springer, Cham, pp. 599–633. https://doi.org/10.1007/978-3-030-02950-0_12.

Hou, M.G., Qu, J.X., Zha, M., Swennen, R., Ding, X.J., Imin, A., Liu, H.L., Bian, B.L., 2022. Significant contribution of haloalkaliphilic cyanobacteria to organic matter in an ancient alkaline lacustrine source rock: a case study from the Permian Fengcheng Formation, Junggar Basin, China. Mar. Petrol. Geol. 138, 105546. https://doi.org/10.1016/j.marpetgeo.2022.105546.

Huang, W.Y., Meinschein, W.G., 1979. Sterols as ecological indicators. Geochem. Cosmochim. Acta 43 (5), 739–745. https://doi.org/10.1016/0016-7037(79)90257-6.

Huang, Y.G., Chen, Z.Q., Wu, S.Q., Feng, X.Q., 2022. Anisian (Middle Triassic) stromatolites from Southwest China: biogeological features and implications for variations of filament size and diversity of Triassic cyanobacteria. Palaeogeogr. Palaeoclimatol. Palaeoecol. 601, 111150. https://doi.org/10.1016/j.palaeo.2022.111150.

Huo, Y.Z., Zhao, W., Zhang, Y.S., Zheng, M.P., Jia, Q.X., Wang, H.X., Lv, G.J., 2005. Plankton community diversity of salt lakes in Xilinguole, Inner Mongolia, China. J. Lake Sci. 17 (3), 243–250 (in Chinese).

Hwang, E.K., Ha, D.S., Baek, J.M., Wee, M.Y., Park, C.S., 2006. Effects of pH and salinity on the cultivated brown alga sargassumfulvellum and associated animals. ChoryuHakhoe-chi/Kor. J. Phycol. 21 (3), 317–321. https://doi.org/10.4490/algae.2006.21.3.317.

Jiang, J.G., Yao, R.H., 1997. Analysis of the biochemical compositions and the β-carotene isomers in five species of Dunaliella. J. S. China Univ. Technol. (Nat. Sci.) 25 (10), 38–41 (in Chinese).

Jiang, Z.S., Fowler, M.G., 1986. Carotenoid-derived alkanes in oils from northwestern China. Org. Geochem. 10 (4–6), 831–839. https://doi.org/10.1016/s0146-6380(86)80020-1.

Johnson, M.E., 2014. Uniformitarianism as a guide to rocky-shore ecosystems in the geological record. Can. J. Earth Sci. 43 (8), 1119–1147. https://doi.org/10.1139/e06-045.

Kang, Y.Y., Xie, W.L., Gao, Y.H., Lin, S.M., Ouyang, L.J., Liu, G.F., 2006. Effect of different concentrations of NaCl and light intensities on β-carotene content in Dunaliella. Plant Physiol. Commun. 42 (2), 315–318 (in Chinese).

Katayama, M., 2022. Fundamental physiological processes: photosynthesis, light-harvesting complex, and carbon-concentrating mechanisms. In: Katayama, M. (Ed.), Cyanobacterial Physiology: from Fundamentals to Biotechnology. Academic Press, pp. 17–28. https://doi.org/10.1016/B978-0-323-96106-6.00013-7.

Klanchui, A., Cheevadhanarak, S., Prommeenate, P., Meechai, A., 2017. Exploring components of the CO2-concentrating mechanism in alkaliphilic cyanobacteria through genome-based analysis. Comput. Struct. Biotechnol. J. 15, 340–350. https://doi.org/10.1016/J.CSBJ.2017.05.001.

Komova, A., Melnikova, A., Namsaraev, Z., Romanov, R., Strakhovenko, V., Ovdina, E., Ermolaeva, N., 2018. Chemical and biological features of the saline Lake Krasnovishnevoye (Baraba, Russia) in comparison with lake Malinovoe (Kulunda, Russia): a reconnaissance study. J. Oceanol. Limnol. 36 (6), 1993–2001. https://doi.org/10.1007/s00343-018-7333-0.

Krienitz, L., Dadheech, P.K., Kotut, K., 2013. Mass developments of the cyanobacteria Anabaenopsis and Cyanospira (Nostocales) in the soda lakes of Kenya: ecological and systematic implications. Hydrobiologia 703 (1), 79–93. https://doi.org/10.1007/s10750-012-1346-z.

Krienitz, L., Schagerl, M., 2016. Tiny and tough: microphytes of East African soda lakes. In: Schagerl, M. (Ed.), Soda Lakes of East Africa. Springer, Cham. https://doi.org/10.1007/978-3-319-28622-8_6.

Li, W.H., Lu, S.F., Tan, Z.Z., He, T.H., 2017. Lacustrine source rock deposition in response to coevolution of paleoenvironment and formation mechanism of organic-rich shales in the Biyang Depression, Nanxiang Basin. Energy Fuel. 31 (12), 13519–13527. https://doi.org/10.1021/acs.energyfuels.7b02880.

Lin, I.I., Hu, C.M., Li, Y.H., Ho, T.Y., Fischer, T.P., Wong, G.T.F., Wu, J.F., Huang, C.W., Chu, D.A., Ko, D.S., Chen, J.P., 2011. Fertilization potential of volcanic dust in the low-nutrient low-chlorophyll western North Pacific subtropical gyre: satellite evidence and laboratory study. Global Biogeochem. Cycles 25 (1), GB1006. https://doi.org/10.1029/2009gb003758.

Liu, G.F., Lou, S.L., You, L.Y., He, B.Y., Lai, R.Q., 1995. A comparative study on the extration of β-carotene and its content of the ten species of Dunaliella (Chlorophyceae). J. Xiamen Univ. 34 (1), 94–98 (in Chinese).

López-Archilla, A.I., Moreira, D., López-García, P., Guerrero, C., 2004. Phytoplankton diversity and cyanobacterial dominance in a hypereutrophic shallow lake with biologically produced alkaline pH. Extremophiles 8 (2), 109–115. https://doi.org/10.1007/s00792-003-0369-9.

Lowenstein, T.K., Jagniecki, E.A., Carroll, A.R., Smith, M.E., Renaut, R.W., Owen, R.B., 2017. The Green River salt mystery: what was the source of the hyperalkaline lake waters? Earth Sci. Rev. 173, 295–306. https://doi.org/10.1016/j.earscirev.2017.07.014.

Ma, J., Cui, X.Q., 2022. Aromatic carotenoids: biological sources and geological implications. Geosyst. Geoenviron. 1 (2), 100045. https://doi.org/10.1016/j.geogeo.2022.100045.

Ma, L., Zhang, Y., Zhang, Z.H., Zhang, G.L., Wang, S.Z., 2020. The geochemical characteristics of the Fengcheng Formation source rocks from the Halaalate area, Junggar Basin, China. J. Petrol. Sci. Eng. 184, 106561. https://doi.org/10.1016/j.petrol.2019.106561.

Marcarelli, A.M., Wurtsbaugh, W.A., Griset, O., 2006. Salinity controls phytoplankton response to nutrient enrichment in the Great Salt Lake, Utah, USA. Can. J. Fish. Aquat. Sci. 63 (10), 2236–2248. https://doi.org/10.1139/f06-113.

Martins, L.L., Schulz, H.-M., Ribeiro, H.J.P.S., Nascimento, C.A. do, Souza, E.S., Cruz, de, da, G.F., 2020. Organic geochemical signals of freshwater dynamics controlling salinity stratification in organic-rich shales in the Lower Permian Irati Formation (Paraná Basin, Brazil). Org. Geochem. 140, 103958. https://doi.org/10.1016/j.orggeochem.2019.103958.

Melack, J.M., Kilham, P., 1974. Photosynthetic rates of phytoplankton in East African alkaline, saline lakes. Limnol. Oceanogr. 19 (5), 743–755. https://doi.org/10.4319/lo.1974.19.5.0743.

Melack, J.M., MacIntyre, S., 2016. Morphometry and physical processes of East African soda lakes. In: Schagerl, M. (Ed.), Soda Lakes of East Africa. Springer, Cham, pp. 61–76. https://doi.org/10.1007/978-3-319-28622-8_3.

Mello, M.R., Koutsoukos, E.A.M., Santos Neto, E.V., Silva Telles Jr., A.C., 1993. Geochemical and micropaleontological characterization of lacustrine and marine hypersaline environments from Brazilian sedimentary basins. In: Katz, B.J., Pratt, L.M. (Eds.), Source Rocks in a Sequence Stratigraphic Framework. American Association of Petroleum Geologists, Yulsa, Ok, pp. 17–34.

Moldowan, J.M., Seifert, W.K., Gallegos, E.J., 1985. Relationship between petroleum composition and depositional environment of petroleum source rocks. AAPG Bull. 69, 1255–1268. https://doi.org/10.1306/ad462bc8-16f7-11d7-8645000102c1865d.

National Energy Administration, 2015. Method of Identification Microscopically the Macerals of Kerogen and Indivision the Kerogen Type by Transmitted-Light and Fluorescence: SY/T 5125-2014. Petroleum Industry Press, Beijing.

Newsted, J.L., 2004. Effect of light, temperature, and pH on the accumulation of phenol by Selenastrum capricornutum, a green alga. Ecotoxicol. Environ. Saf. 59 (2), 237–243. https://doi.org/10.1016/j.ecoenv.2003.07.009.

Oberholster, P.J., Botha, A.M., Ashton, P.J., 2009. Appearance of new taxa: invertebrates, phytoplankton and bacteria in an alkaline, saline, meteorite crater lake, South Africa. Fund. Appl. Limnol. 174 (3), 271–282. https://doi.org/10.1127/1863-9135/2009/0174-0271.

Ogbesejana, A.B., Bello, O.M., Akintade, O.O., Jacob, A.G., Odusina, B.O., 2022. Geochemical appraisal of crude oils from Niger Delta Basin, Nigeria: insights from β-carotane, rearranged hopanes, tricyclic terpanes, tetracyclic terpanes, and phenyldibenzofurans. Arabian J. Geosci. 15, 1244. https://doi.org/10.1007/s12517-022-10501-y.

Omodeo-Salé, S., Suárez-Ruiz, I., Arribas, J., Mas, R., Martínez, L., Josefa Herrero, M., 2016. Characterization of the source rocks of a paleo-petroleum system (Cameros Basin) based on organic matter petrology and geochemical analyses. Mar. Petrol. Geol. 71, 271–287.

Opiyo, S., 2020. Assessment of the temporal and spatial variability in the phytoplankton dynamics of a tropical alkaline-saline lake Simbi, Kenya. Int. Res. J. Environ. Sci. 9, 14–23.

Patias, L.D., Fernandes, A.S., Petry, F.C., Mercadante, A.Z., Jacob-Lopes, E., Zepka, L.Q., 2017. Carotenoid profile of three microalgae/cyanobacteria species with peroxyl radical scavenger capacity. Food Res. Int. 100, 260–266. https://doi.org/10.1016/j.foodres.2017.06.069.

Pecoraino, G., D'Alessandro, W., Inguaggiato, S., 2015. The other side of the coin: geochemistry of alkaline lakes in volcanic areas. In: Rouwet, D., Christenson, B., Tassi, F., et al. (Eds.), Volcanic Lakes. Advances in Volcanology. Springer, Berlin, Heidelberg, pp. 219–237. https://doi.org/10.1007/978-3-642-36833-2_9.

Pennington, F., Guillard, R.R.L., Liaaen-Jensen, S., 1988. Carotenoid distribution patterns in Bacillariophyceae (diatoms). Biochem. Systemat. Ecol. 16 (7–8), 589–592. https://doi.org/10.1016/0305-1978(88)90067-1.

Peters, K.E., Walters, C.C., Moldowan, J.M., 2005. The biomarker guide. In: Biomarkers & Isotopes in Petroleum Systems & Earth History, vol. 2. University Press, Cambridge.

Pick, U., 2002. Adaptation of the halotolerant alga Dunaliella to high salinity. In: Läuchli, A., Lüttge, U. (Eds.), Salinity: Environment - Plants - Molecules. Springer, Dordrecht, pp. 97–112. https://doi.org/10.1007/0-306-48155-3_5.

Rippen, D., Littke, R., Bruns, B., Mahlstedt, N., 2013. Organic geochemistry and petrography of Lower Cretaceous Wealden black shales of the Lower Saxony Basin: the transition from lacustrine oil shales to gas shales. Org. Geochem. 63, 18–36. https://doi.org/10.1016/j.orggeochem.2013.07.013.

Salm, C.R., Saros, J.E., Martin, C.S., Erickson, J.M., 2009. Patterns of seasonal phytoplankton distribution in prairie saline lakes of the northern Great Plains (U.S.A.). Saline Syst. 5 (1). https://doi.org/10.1186/1746-1448-5-1, 1–1.

Schagerl, M., Renaut, R.W., 2016. Dipping into the Soda Lakes of East Africa. In: Schagerl, M. (Ed.), Soda Lakes of East Africa. Springer, Cham, pp. 3–24. https://doi.org/10.1007/978-3-319-28622-8_1.

Schopf, J.W., 2012. The Fossil Record of Cyanobacteria. In: Whitton, B. (Ed.), Ecology of Cyanobacteria II. Springer, Dordrecht, pp. 15–31. https://doi.org/10.1007/978-94-007-3855-3_2.

Schouten, S., Damsté, J.S.S., Baas, M., Dalen, A.C.K.-V., Kohnen, M.E.L., Leeuw, J.W.D., 1995. Quantitative assessment of mono- and polysulphide-linked carbon skeletons in sulphur-rich macromolecular aggregates present in bitumens and oils. Org. Geochem. 23 (8), 765–775. https://doi.org/10.1016/0146-6380(95)00055-j.

Sili, C., Torzillo, G., Vonshak, A., 2012. Arthrospira (Spirulina). In: Whitton, B. (Ed.), Ecology of Cyanobacteria II. Springer, Dordrecht. https://doi.org/10.1007/978-94-007-3855-3_25.

Sinninghe Damste, J.S., Kenig, F., Koopmans, M.P., Koster, J., Schouten, S., Hayes, J.M., De Leeum, J.W., 1995. Evidence for gammacerane as an indicator of water column stratification. Geochem. Cosmochim. Acta 59 (9), 1895–1900. https://doi.org/10.1016/0016-7037(95)00073-9.

Summons, R.E., Jahnke, L.L., Hope, J.M., Logan, G.A., 1999. 2-Methylhopanoids as biomarkers for cyanobacterial oxygenic photosynthesis. Nature 400 (6744), 554–557. https://doi.org/10.1038/23005.

Tang, Y., He, W.J., Bai, Y.B., Zhang, X., Zhao, J.Z., Yang, S., Wu, H.Y., Zou, Y., Wu, W.T., 2021. Source rock evaluation and hydrocarbon generation model of a permian alkaline lakes—a case study of the Fengcheng formation in the Mahu Sag, Junggar basin. Minerals 11 (6), 644. https://doi.org/10.3390/min11060644.

Tao, K.Y., Cao, J., Chen, X., Nueraili, Z., Hu, W.X., Shi, C.H., 2019. Deep hydrocarbons in the northwestern Junggar Basin (NW China): Geochemistry, origin, and implications for the oil vs. gas generation potential of post-mature saline lacustrine source rocks. Mar. Petrol. Geol. 109, 623–640. https://doi.org/10.1016/j.marpetgeo.2019.06.041.

Tran, Q.G., Cho, K., Kim, U., Yun, J.H., Cho, D., Heo, J., Park, S.B., Kim, J.W., Lee, Y.J., Ramanan, R., Kim, H.S., 2019. Enhancement of β-carotene production by regulating the autophagy-carotenoid biosynthesis seesaw in Chlamydomonas reinhardtii. Bioresour. Technol. 292, 121937. https://doi.org/10.1016/j.biortech.2019.121937.

Tu, J., Chen, J., Zhang, D., Cheng, K., Chen, J., Yang, Z., 2012. A petrographic classification of macerals in lacustrine carbonate source rocks and their organic petrological characteristics: A case study on Jiuxi basin, NW China. Acta Petrol. Sin. 28, 917–926.

Vareschi, E., 1987. Saline Lake Ecosystems. Springer, Berlin, Heidelberg.

Wacey, D., 2013. Early Life on Earth. Springer, Netherlands. https://link.springer.com/book/10.1007%2F978-1-4020-9389-0.

Wang, G.B., Wang, Y., Li, E.T., Li, J., Huang, P., Xu, H., Yu, S., Pan, C.C., 2017. Molecular and carbon isotopic compositions of oil components in the Baikouquan Formation oil-bearing reservoir rocks on the western slope of the Mahu Sag, Junggar Basin. Geochimica 46 (3), 276–291 (in Chinese).

Wang, S.M., Dou, H.S., 1998. Lake Records of China. Science Press, Beijing (in Chinese).

Wang, T.T., Cao, J., Jin, J., Xia, L.W., Xiang, B.L., Ma, W.Y., Li, W.W., He, W.J., 2021. Spatiotemporal evolution of a Late Paleozoic alkaline lake in the Junggar Basin, China. Mar. Petrol. Geol. 124, 104799. https://doi.org/10.1016/j.marpetgeo.2020.104799.

Wang, Y.C., Cao, J., Tao, K.Y., Xiao, W.Y., Xiang, B.L., Li, E.T., Pan, C.C., 2022. Absence of β-carotane as proxies of hydrothermal activity in brackish lacustrine sediments. Palaeogeogr. Palaeoclimatol. Palaeoecol. 587, 110801. https://doi.org/10.1016/j.palaeo.2021.110801.

Wei, W., Algeo, T.J., Lu, Y.B., Lu, Y.C., Liu, H.M., Zhang, S.P., Peng, L., Zhang, J.Y., Chen, L., 2018. Identifying marine incursions into the Paleogene Bohai Bay Basin lake system in northeastern China. Int. J. Coal Geol. 200, 1–17. https://doi.org/10.1016/j.coal.2018.10.001.

White, A.H., Youngs, B.C., 1980. Cambrian alkali playa-lacustrine sequence in the northeastern Officer Basin, South Australia. J. Sediment. Res. 50, 1279–1286. https://doi.org/10.1306/212f7bd0-2b24-11d7-8648000102c1865d.

Windley, B.F., 1993. Uniformitarianism today: plate tectonics is the key to the past. J. Geol. Soc. London. 150 (1), 7–19. https://doi.org/10.1144/gsjgs.150.1.0007.

Wu, J., 2018. The more toxic the East African Salt Lake is, the more beautiful it is. Chin. Nat. Geogr. 7, 26–36 (in Chinese).

Wu, W.W., 2012. Effect of Environmental Factors and Inhibitors on Fatty Acid Biosynthesis in Phaeodactylum Tricornutum. Dissertation for the Degree of Master. Nanjing Agricultural University, Nanjing (in Chinese).

Wu, X.Q., Jiang, J.Q., Hu, J.Y., 2013. Determination and Occurrence of Retinoids in a Eutrophic Lake (Taihu Lake, China): Cyanobacteria Blooms Produce Teratogenic Retinal. Environ. Sci. Technol. 47 (2), 807–814. https://doi.org/10.1021/es303582u.

Xia, L.W., Cao, J., Bian, L.Z., Hu, W.X., Wang, T.T., Zhi, D.M., Tang, Y., Li, E.T., 2022. Co-evolution of paleo-environment and bio-precursors in a Permian alkaline lake, Mahu mega-oil province, Junggar Basin: Implications for oil sources. Sci. China Earth Sci. 65 (3), 462–476. https://doi.org/10.1007/s11430-021-9861-4.

Xia, L.W., Cao, J., Hu, W.H., Zhi, D.M., Tang, Y., Li, E.T., He, W.J., 2021. Coupling of paleoenvironment and biogeochemistry of deep-time alkaline lakes: A lipid biomarker perspective. Earth Sci. Rev. 213, 103499. https://doi.org/10.1016/j.earscirev.2020.103499.

Xia, L.W., Cao, J., Stüeken, E.E., Zhi, D.M., Wang, T.T., Li, W.W., 2020. Unsynchronized evolution of salinity and pH of a Permian alkaline lake influenced by hydrothermal fluids: A multi-proxy geochemical study. Chem. Geol. 541, 119581. https://doi.org/10.1016/j.chemgeo.2020.119581.

Yang, F., 2014. Characteristics of Community Structures of Phytoplankton and Protozoa in the Salt Lakes, Tibet. Dissertation for the Degree of Master. Shanghai Ocean University, Shanghai (in Chinese).

Yang, H., Chen, Z.Q., Papineau, D., 2022. Cyanobacterial spheroids and other biosignatures from microdigitate stromatolites of Mesoproterozoic Wumishan Formation in Jixian, North China. Precambrian Res. 368, 106496. https://doi.org/10.1016/j.precamres.2021.106496.

Yang, W.S., Zhang, Y., Wang, Z.X., Zhu, C.L., Song, L.W., Han, X.H., Sun, D.L., 2008. Investigation and study on aquatic life in the Wu Lan Nord Lake of Inner Mongolia. J. Inn. Mong. Agric. Univ. (Nat. Sci. Ed.) 29 (2), 8–11 (in Chinese).

Yawanarajah, S.R., Kruge, M.A., Mastalerz, M., Sliwinski, W., 1993. Organic geochemistry of Permian organic-rich sediments from the Sudetes area, SW Poland. Org. Geochem. 20 (2), 267–281. https://doi.org/10.1016/0146-6380(93)90044-c.

Yu, K.H., Cao, Y.C., Qiu, L.W., Sun, P.P., 2019. Depositional environments in an arid, closed basin and their implications for oil and gas exploration: The lower Permian Fengcheng Formation in the Junggar Basin, China. AAPG Bull. (Arch. Am. Art) 103 (9), 2073–2115. https://doi.org/10.1306/01301917414.

Yu, K.H., Zhang, Z.J., Cao, Y.C., Qiu, L.W., Zhou, C.M., Cheng, D.W., Sun, P.P., Yang, Y.Q., 2021. Origin of biogenic-induced cherts from Permian alkaline saline lake deposits in the NW Junggar Basin, NW China: Implications for hydrocarbon exploration. J. Asian Earth Sci. 211, 104712. https://doi.org/10.1016/j.jseaes.2021.104712.

Yuan, J.P., Zhang, Y.M., Shi, X.M., Gong, X.D., Chen, F., 1997. Simultaneous Determination of Caotenoids and Chlorophylls in Algae by High Performance Liquid Chromatography. Chin. J. Chromatogr. 15 (2), 133–135 (in Chinese).

Zhang, Y.X., Xu, C., 2019. Study on the hydrocarbon generation potential and biomarker characteristics of the Paleogene in Dongpu Sag. J. Geol. Univ. 25, 813–822 (in Chinese).
Zhang, Z.D., Gu, Y.L., Jin, J., Li, E.T., Yu, S., Pan, C.C., 2022. Assessing source and maturity of oils in the Mahu sag, Junggar Basin: Molecular concentrations, compositions and carbon isotopes. Mar. Petrol. Geol. 141, 105724. https://doi.org/10.1016/j.marpetgeo.2022.105724.
Zhang, Z.J., Yuan, X.J., Wang, M.S., Zhou, C.M., Tang, Y., Chen, X.Y., Lin, M.J., Cheng, D.W., 2018. Alkaline-lacustrine deposition and paleoenvironmental evolution in Permian Fengcheng Formation at the Mahu sag, Junggar Basin, NW China. Petrol. Explor. Dev. 45 (6), 1036–1049. https://doi.org/10.1016/s1876-3804(18)30107-1.
Zhao, W., 2010. Salt Lake Ecology in China. Science Press, Beijing (in Chinese).
Zheng, C.L., 2015. The Influence of Media Ingredients and Ph on the Growth of Chloromonas Rosae Var. Psychrophila. Theses and Dissertations–Biosystems and Agricultural Engineering. University of Kentucky, Lexington.
Zheng, M.P., Zhao, Y.Y., Liu, J.Y., 1998. Quaternary Saline Lake deposition and Paleoclimate. Quat. Sci. 14 (4), 298–307 (in Chinese).